# TECHNICAL REPORT No. 33

# NUMERICAL SIMULATIONS OF A CASE OF BLOCKING: THE EFFECTS OF OROGRAPHY AND LAND-SEA CONTRAST

by

L. R. Ji* and S. Tibaldi

September 1982

* *On leave from the*
*Institute of Atmospheric Physics, Academia Sinica, Beijing, China*

C O N T E N T S PAGE

**Abstract**

The North-Atlantic Blocking case of 17-30 December 1978 is briefly described synoptically and the results from several numerical 10 days global integrations are investigated to assess the role played in both onset and maintenance of the block by the model's global orography, by the Rocky Mountains and by the Tibetan Plateau separately, by the surface exchanges (land-sea contrast) and by the model's physical parameterizations. A highly simplified analytical model of flow over the Rockies is also presented that explains some features evidentiated by the numerical experiments. Despite the limitations of a single case study, some efforts are made to bridge the gap between oversimplified numerical models and observational diagnostic studies.

## 1. INTRODUCTION

Atmospheric blocking is a typical large-scale weather situation ("Grosswetterlage") mainly characterized by its meridional extent and time persistence. Its establishment or decay usually brings about a marked change of hemispheric circulation and its persistence is associated with pronounced deviations from climatology. The study of blocking being therefore both theoretically and practically important, it has received long-standing attention.

The first attempts to investigate this problem can be traced back as far as the late 1940's and early 1950's (e.g. Berggren et al, 1949; Rossby, 1949; Yeh, 1949; Rex, 1950a and 1950b). Later, the closely connected problems of the dynamics of ultra-long waves and of stratospheric sudden warmings have attracted considerable interest. Recently, there has been renewed interest in blocking dynamics, both through linear or non-linear theoretical approaches (Egger, 1978; Tung and Lindzen, 1979; Charney and de Vore, 1979; Källén, 1980). For a more comprehensive review of theories on blocking, the reader is referred to Bengtsson (1979).

Regarding the mechanism responsible for the development of blocking, some authors considered that it could mainly result from intense baroclinic instability (Yeh and collaborators, 1962; Namias, 1964). This would be consistent with the hypothesis that the energy of the ultra-long waves seems to stem from the conversion of available potential energy (Wiin-Nielsen et al, 1963). Other authors have concentrated their attention more on the asymmetry of atmospheric forcings and have related this to the geographical distribution of blocking frequency (Egger, 1978; Tung and Lindzen, 1979). Egger (1978) suggested that blocking can result from the interaction of forced waves and moving free waves, while Tung and Lindzen (1979) proposed a resonant type mechanism. However, the link between these two aspects has not been fully clarified yet (Chen, 1979). Although the effect of orography has been widely emphasized, its relative role compared to land-sea contrast in the dynamics of blocking is still ambiguous. The results of numerical experiments by Everson and Davies (1970) showed that only the existence of longitudinal land-sea temperature differential led to blocking. White and Clark (1975) stressed the importance of land-sea thermal contrasts in making it easier for the ultra-long waves to become baroclinically unstable. Tung and Lindzen (1979) argued that the sea surface temperature can play a constructive rather than destructive role only when a climatologically abnormal distribution of SST occurs, while Kikuchi (1971) showed that land-sea contrast alone accounts for a small proportion of the distribution of frequency of blocking occurrence.

The present study is attempting to assess the relative importance of these forcings and how they play their part during a real blocking situation, using a numerical simulation of the occurrence. The link between the forcings and the stability properties inherent to the atmosphere will also be discussed.

Most numerical experiments intended to simulate blocking have been initiated from an idealized state and/or conducted by highly simplified models (e.g. Egger, 1978; Kikuchi, 1971; Kalnay-Rivas and Merkine, 1981). An alternative approach is discussed in Bengtsson (1981), where a sophisticated GCM has been used on real global initial conditions. This approach is intended to give a more realistic representation of atmospheric blocking. The present study also pursues this way of attack. Using the ECMWF grid point model (Burridge and Haseler, 1977, Tiedtke et al, 1979) a series of ten day forecasts for the 17 Dec, 1978 case have been performed using different model configurations and surface boundary conditions (forcing).

Section 2 contains a brief general synoptic description of the case study, while Sections 3 to 6 describe the experiments in detail. Section 7 contains an attempt, through a very simple analytical approach, to explain how a large-scale orographic feature like the Rocky Mountains can favour the onset and maintenance of blocking.

## 2. THE SELECTED CASE: THE BLOCKING SITUATION OF 17-30 DECEMBER 1978

This is a typical case of Atlantic blocking (see Fig. 1), the formation and persistence of which give rise to a spell of severe cold weather in the north-west of Europe. It is a "meridional type" blocking, as classified by Sumner (1954). The event begins with the intense development of a low on the east coast of North America (Fig. 1a), the maximum pressure drop for 24 hours being 34 dams at 500 mb and 31 mb at the surface. The typical blocking flow pattern establishes around day 5 of the forecast, showing all the main features described by Rex (1950a and 1950b). Noticeable are the huge high and two branches of the split jet, especially the one to the north (Fig. 1c,d). The centre of the high remains nearly at the same position, (east of Greenland, around 30°W, 70°N) from day 5 to day 10. Afterwards, it slowly moves to the west weakening and dying away, but still persisting for another three days.

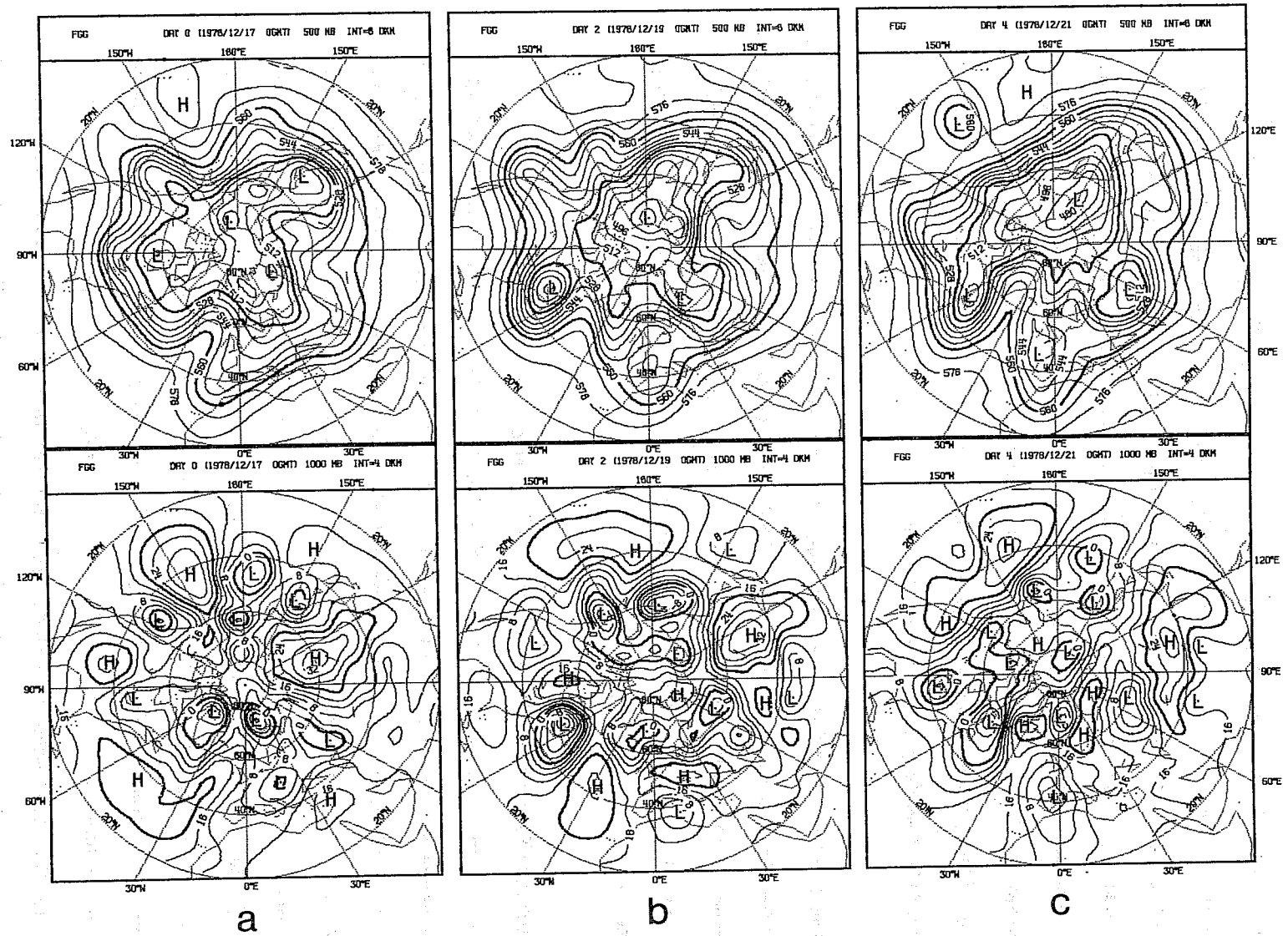


Fig. 1 ECMWF FGGE analyses for (a) 00 GMT 17 December 1978 (initial conditions for all numerical experiments), (b) 00 GMT 19 December, (c) 00 GMT 21 December; referred to as day 0, 2 and 4 respectively. Upper: 500 mb height drawn every 8 dam. Lower: 1000 mb height drawn every 4 dam.

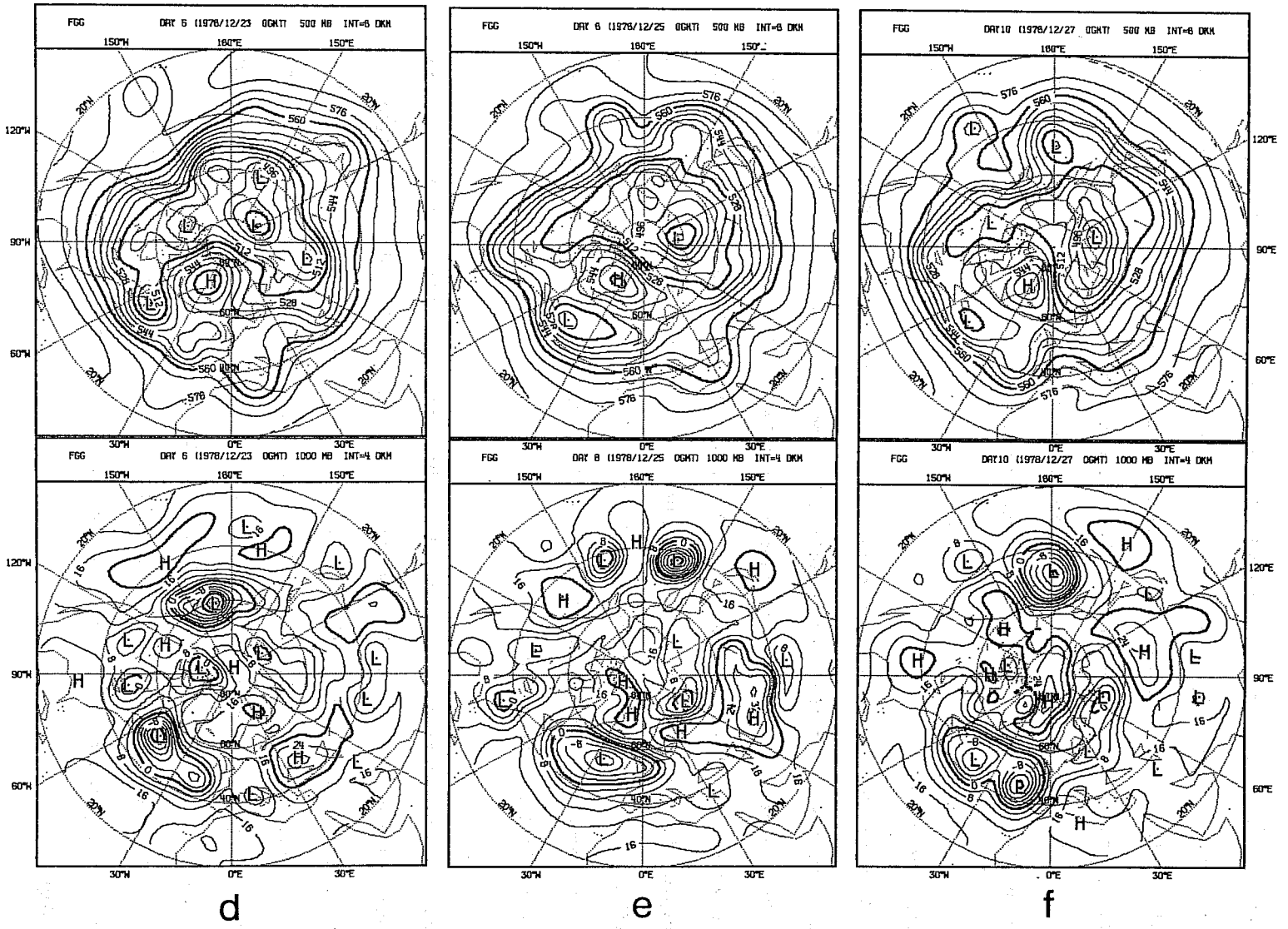


Fig. 1 (contd.) ECMWF FGGE analyses for (d) 00 GMT 23 December 1978, (e) 00 GMT 25 December, (f) 00 GMT 27 December, referred to as day 6, 8 and 10 respectively. Upper: 500 mb height drawn every 8 dam. Lower: 1000 mb height drawn every 4 dam.

A major change of circulation of the whole northern hemisphere accompanies the build-up of the block; a pre-existing relatively zonal flow over the Atlantic area completely breaks down. Over Eurasia, on the contrary, a transition from a meridional pattern to dominating westerlies occurs and the centre of polar vortex moves to be situated over Asia (Fig. 1d). The success or failure to represent these conspicuous changes will be the basis for the following discussion of the numerical experiments.

## 3. THE CONTROL RUN

Table 1 lists the characteristics of all the experiments performed. The table shows also a "useful predictability" parameter which shows the time at which the anomaly correlation of geopotential height (averaged over 1000-200 mb and 20°-85°N) degrades to 0.6. The value 0.6, although arbitrary in principle, is used following Hollingsworth et al (1980). We will first describe Exp.F81, the control run, that includes orography and land-sea contrast together with all model physics (Tiedtke et al, 1979) and will serve as the basis for comparison.

The control run is also characterized by the highest objective skill of all the experiments. Synoptically, as can be seen in Fig. 2 and 3, it captures the main features of the blocking episode, such as the splitting of the jet, the separation and position of the high-low pressure doublet and the ensuing drastic change of circulation pattern over Eurasia. Even up to day 8 the predicted chart shows a good resemblance to the observed. Obvious drawbacks are an underestimation of the intensity of the high pressure cell and a considerable phase error in the positioning of the blocking feature from day 8 to day 10.

If we look at the Hovmöller diagram for the 10 day period (Fig. 3), we can see that after the intense development of the off-coast low and downstream

| Experiment | | Mountains | Land/Sea Contrast? | Remarks | Is observed blocking reproduced? | | Useful predictability (days) | | |
|---|---|---|---|---|---|---|---|---|---|
| Exp.Name | Related Fig.No. | | | | Onset | Maintenance | Total 0-20 | WN 1-3 | WN 4-9 |
| F81 | 2 | Yes | Yes | Control Experiment "Physics" all included | Yes | Yes | 5.5 | 6.8 | 4.8 |
| G07 | 6 | No | Yes | "Physics" all included | No | No | 4.3 | 4.6 | 4.3 |
| G14 | 10 | No Tibet | Yes | "Physics" all included | Yes | Yes | 4.9 | 6.1 | 4.6 |
| G63 | 11 | No Rockies | Yes | "Physics" all included | No | No | 4.5 | 5.0 | 4.2 |
| G16 | 13 | Yes | No (all sea) | "Physics" all included $Z_o$=.2m; $q_*$=.01; $T_*=T_{15}$ | Yes | No(?) | 5.0 | 6.8 | 4.8 |
| F98 | 17 | No | No (all sea) | Minimum physics run: dry adiabatic readj; weak surface friction and internal diffusion only | Yes | No | 3.6 | 3.6 | 3.7 |
| I14 | 18 | Yes | No (all sea) | Minimum physics run: dry adiabatic readj., weak surface friction and internal diffusion only | Yes | Yes(?) | 4.3 | 5.2 | 4.1 |

**Table 1** List of all experiments discussed and of their characteristics. $Z_o$ indicates the roughness length of the model's surface, $q_*$ the surface soil moisture, $T_*$ the surface temperature, $T_{15}$ the temperature of the lowermost model level (level 15).

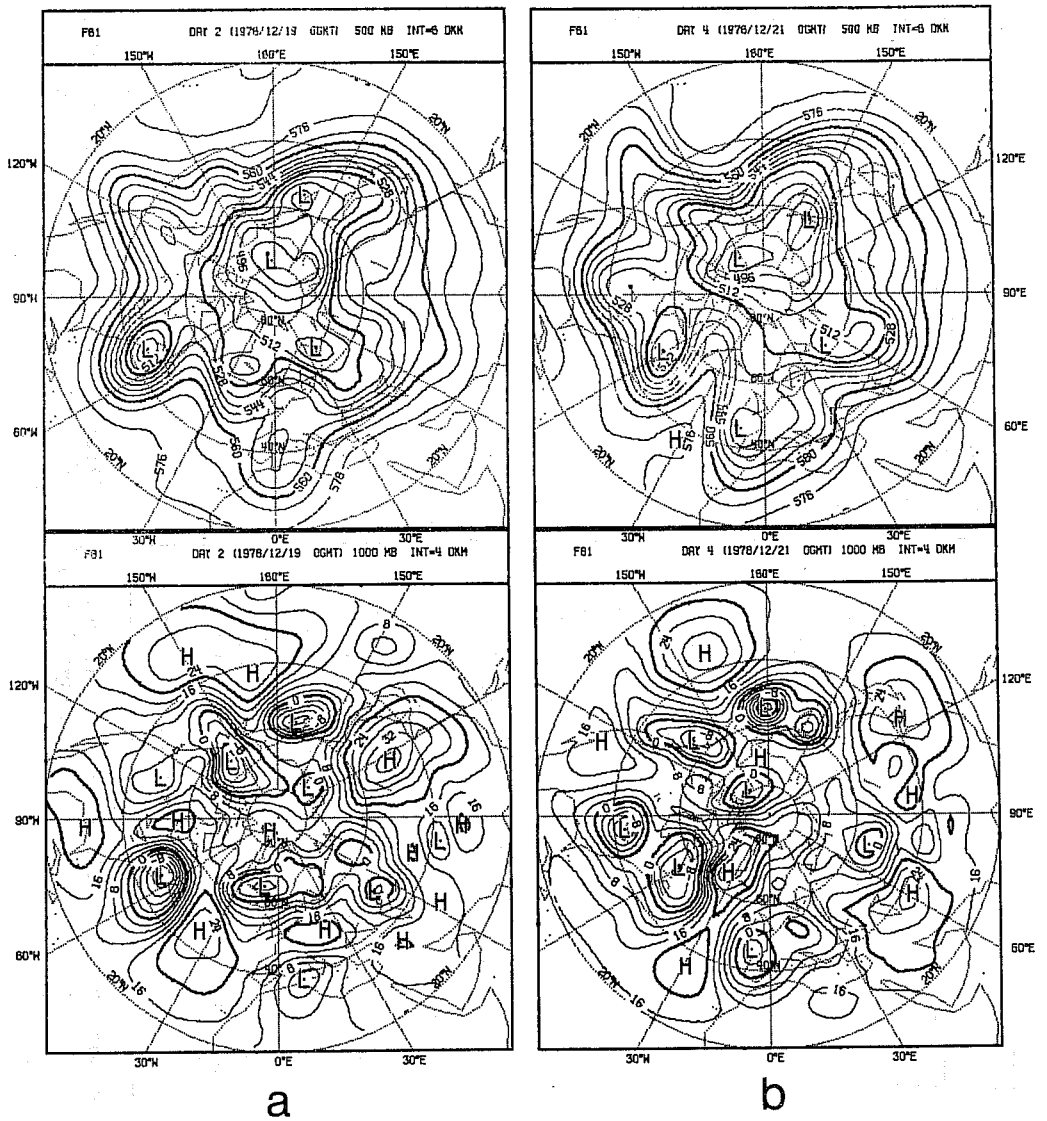


Fig. 2 Model run F81 (control) for (a) day 2, (b) day 4.
Upper: 500 mb height drawn every 8 dam.
Lower: 1000 mb height drawn every 4 dam.

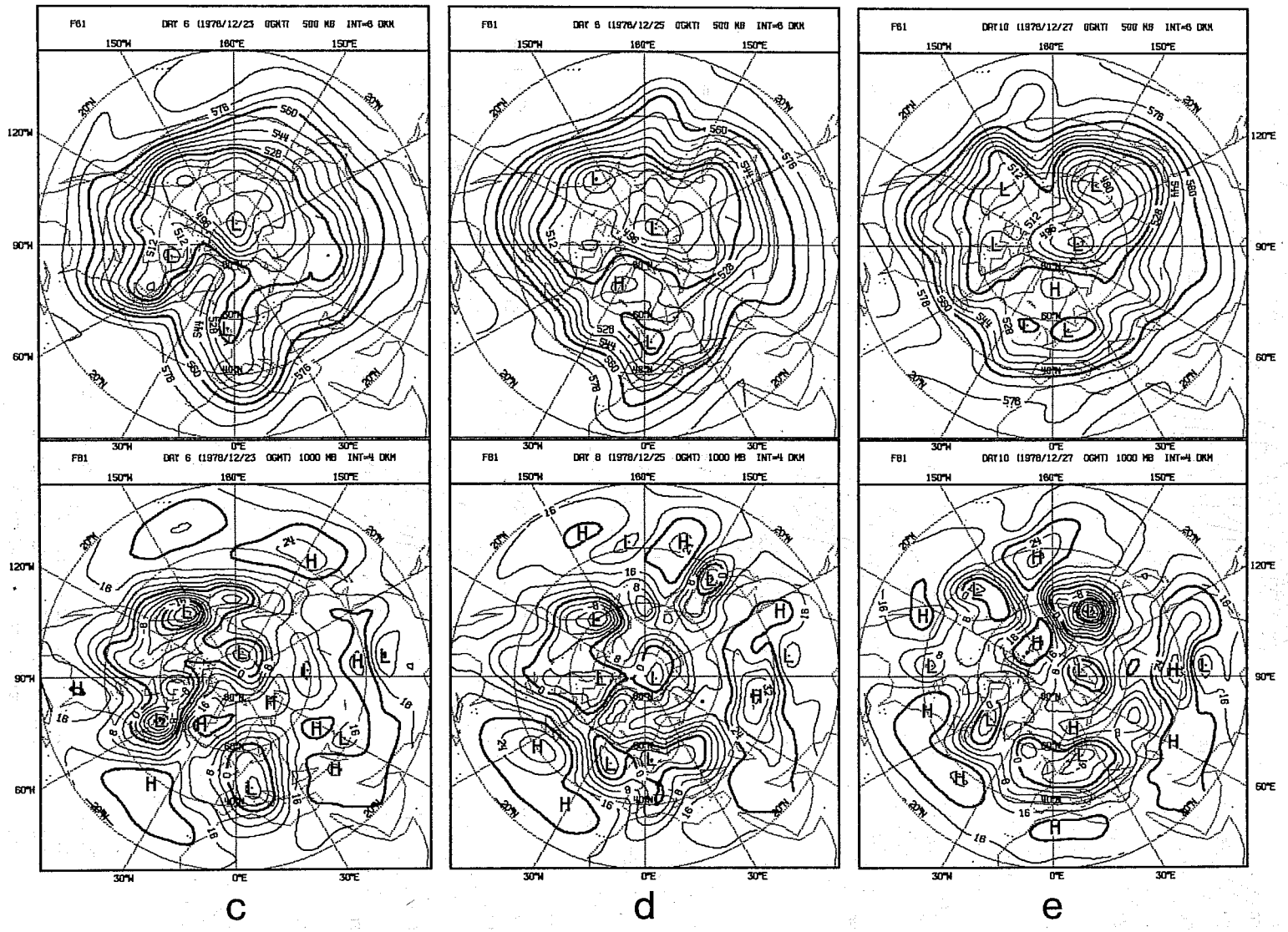


Fig. 2 (contd.) Model run F81 (control) for (c) day 6, (d) day 8, (e) day 10.
Upper: 500 mb height drawn every 8 dam. Lower: 1000 mb height drawn every 4 dam.

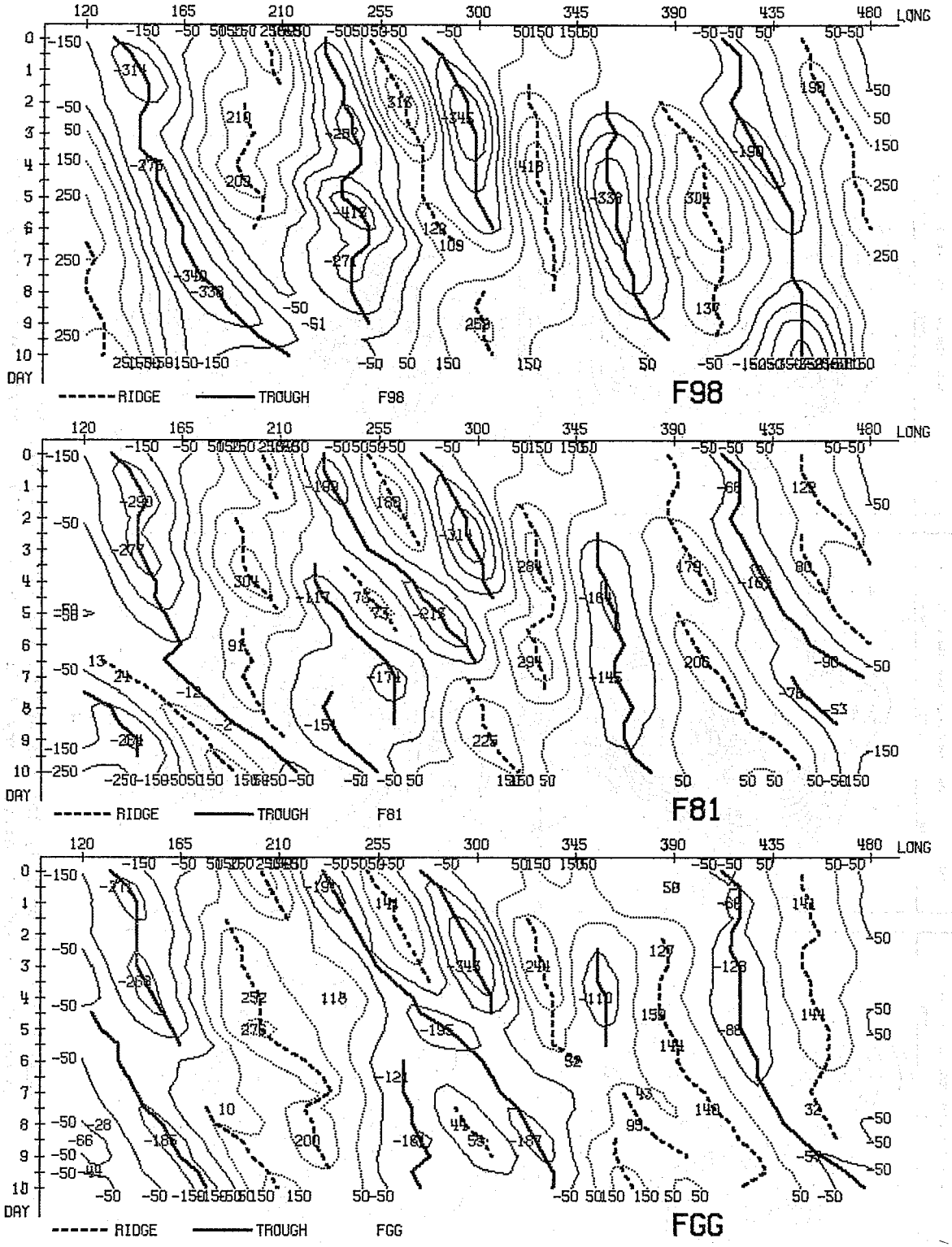


Fig. 3 Hovmöller diagrams of 500 mb geopotential height for wavenumber 1 to 9 waveband averaged for 35°N-55°N. FGG: verifying analysis. F81: control run. F98: minimum physics run. Vertical axes show time, horizontal axes longitude.

ridge, there are two successive troughs coming up and developing in the same region as the previous slow dying trough, that is between 90°W and 60°W. Each of these trough developments results in a nearly in-phase interaction between the transient and the standing features. A point worth mentioning is that the evolution phase of these transient wave packets are under the influence or control of the orography,and in this sense they are also partially "forced" rather than completely "free". This seems to contribute to the maintenance of the block: we will come back to this point later.

It is interesting to investigate the energetics throughout the 10 day period (Fig. 4). During the early part of the set-up phase of the blocking, an increase of kinetic energy (KE) takes place in the wavenumber band 4 to 9. On day 3, the KE of this band shows a sharp decrease, offset by an increase of KE for the wavenumber band 1 to 3. The forecast shows a similar behaviour of energetics, though the increase of KE for wavenumbers 1-3 is weaker. This suggests that the ultra-long waves during a blocking situation might receive a considerable part of their KE from non-linear interaction with long waves rather than simply from direct baroclinic instability of the ultra-long waves themselves, (White and Clark, 1975). This result is, in this respect, somewhat different from the case investigated by Bengtsson (1981) where the amplitude of the ultra-long waves was reduced during the build-up of the blocking*.

---

*It has been brought to the attention of the authors that diagnostics results, based on observations, presented in an independent work on this same blocking development by Hansen and Chen (1982) are in very good agreement with our findings on the energetic behaviour and energetic exchange between wavenumber bands. We are grateful to A.Simmons for pointing this out to us.

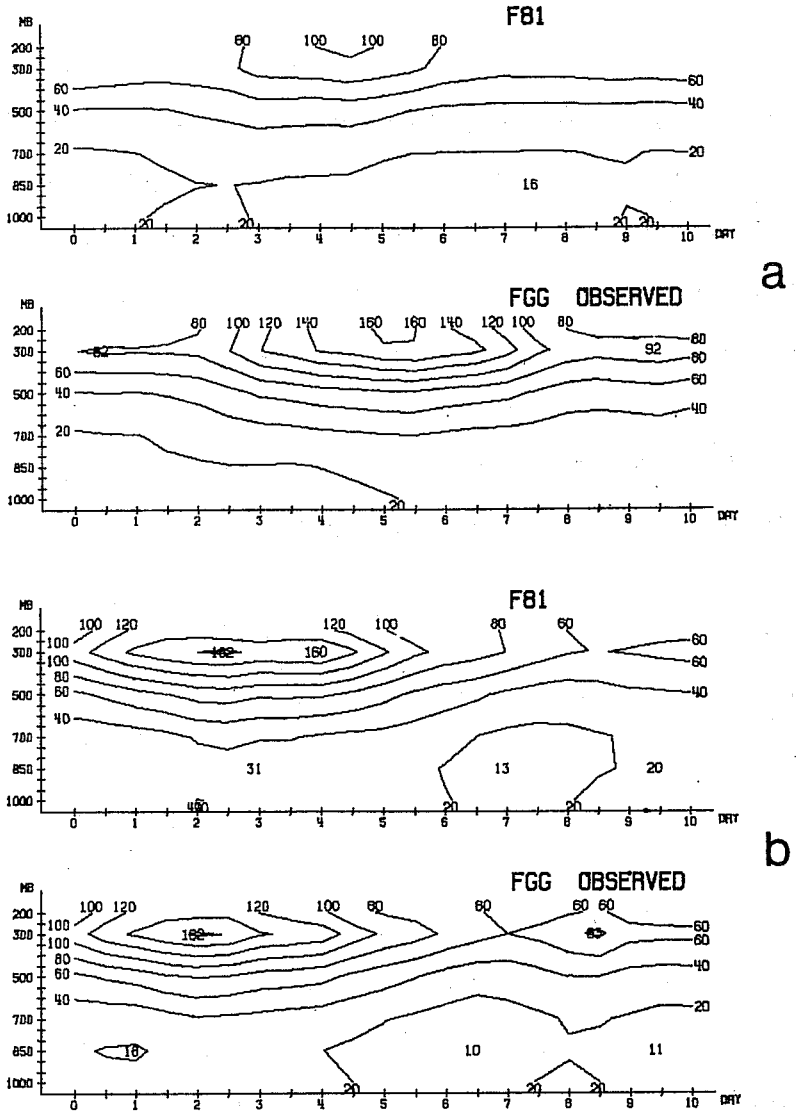


Fig. 4 Time-height variation of mean kinetic energy for Northern Hemisphere calculated from geostrophic wind for F81 (control run) and FGG (verifying analysis). Upper: for wavenumbers 1-3 (a). Lower: for wavenumbers 4-9 (b)

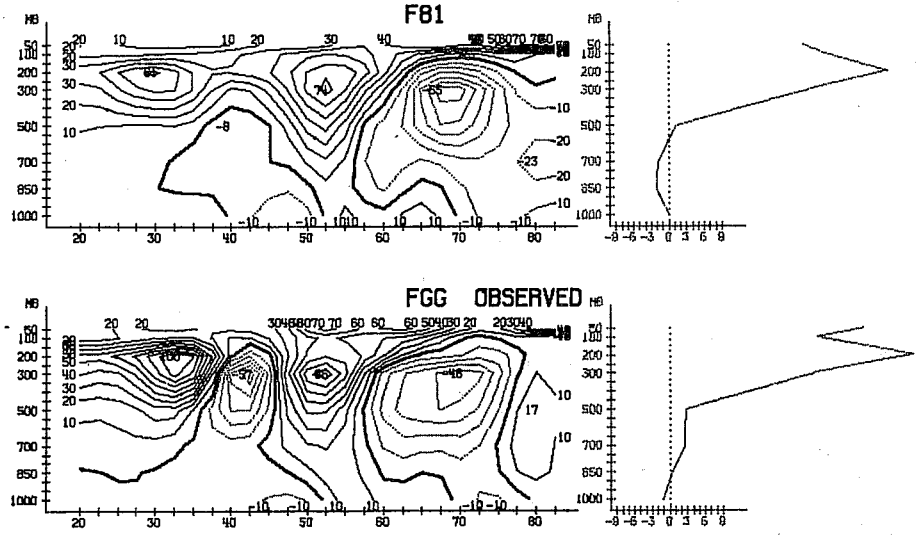


Fig. 5 Vertical cross section of momentum flux as a function of latitude at day 2 for F81 (control run) and FGG (verifying analysis). Units: $m^2s^{-2}$.

It is also interesting to note that during the early stages (day 2) the latitudinal distribution of momentum flux (Fig. 5 ) shows two convergence zones at about 35°N and 60°N respectively which seem to indicate the build-up of separate branches of the jet. The forecast is successful in capturing this aspect of the development.

## 4. THE INFLUENCE OF OROGRAPHY

### 4.1 The experiment without mountains

This section will concentrate on the effect of orography. Exp.G07 was run with the same model as the control experiment but without mountains. This comparison should therefore highlight the global effects of orography. Fig. 6 shows clearly that, although the first few days of forecast look similar, the differences that develop during the integration are very large as should be expected. The ridge over the Atlantic is completely missing, instead, a ridge over North America appears and develops into a blocking-like pattern at day ten. This perhaps fortuitous event suggests that the inherent atmospheric baroclinity coupled with land-sea constrast effects might be enough to produce blocking-like situations, but more or less as free-running modes. The regional preference or the phase-locking action on the ultra-long waves seems to be a main attribute of the orography rather than of the land-sea contrast. If we look at the Hövmoller diagram for wavenumbers 1 to 3 (Fig. 7), we can see this more clearly. The ultra-long wave components move eastward in the no-mountain run, while in the control run they remain, by and large, at the same longitude as the observed ones. Consequently, the deterioration of forecast skill for this run comes mainly from the wavenumber 1 to 3 components (see Table 1).

Some more regional characteristics connected to the Rockies can also be noticed observing the daily difference maps. Fig. 8 shows the day 2 and 4 difference maps; a time, therefore, when the blocking has not yet become established. Two belts of opposite sign stretching to the east of the

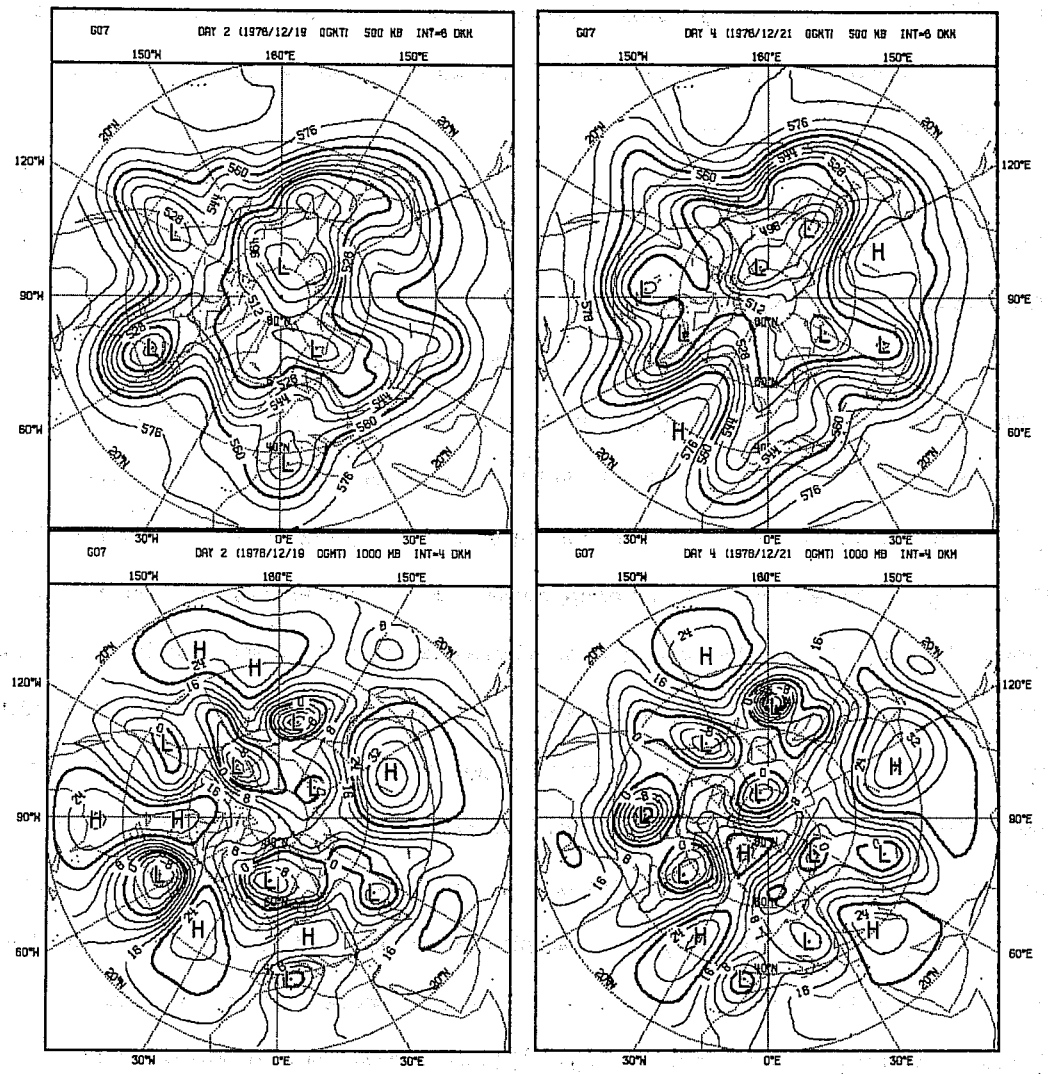


Fig. 6 Model run G07 (no mountain run). (a) day 2, (b) day 4. Upper: 500 mb height drawn every 8 dam. Lower: 1000 mb height drawn every 4 dam.

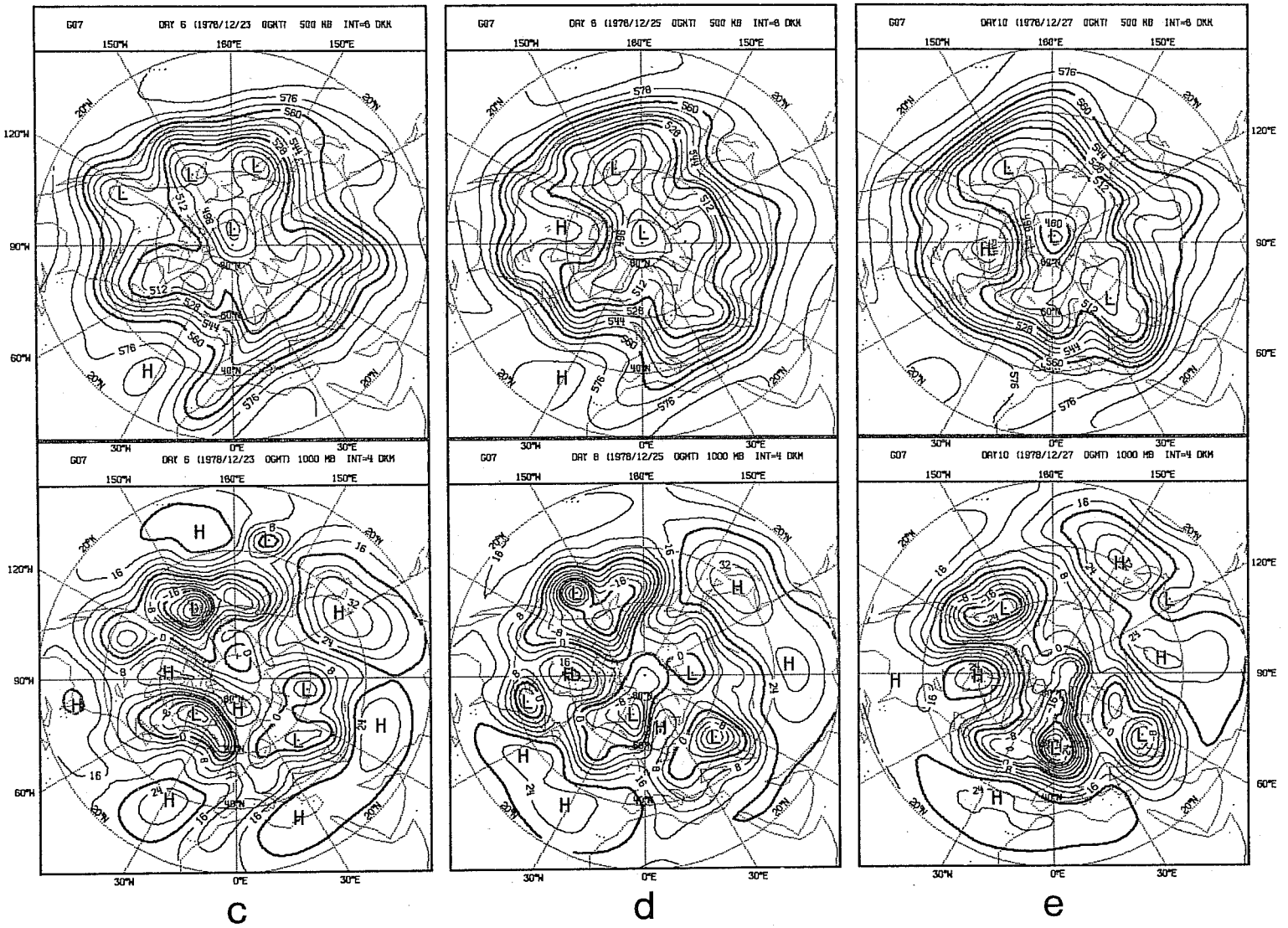


Fig. 6 (contd.) Model run G07 (no mountain run). (c) day 6, (d) day 8, (e) day 10. Upper: 500 mb height drawn every 8 dam. Lower: 1000 mb height drawn every 4 dam.

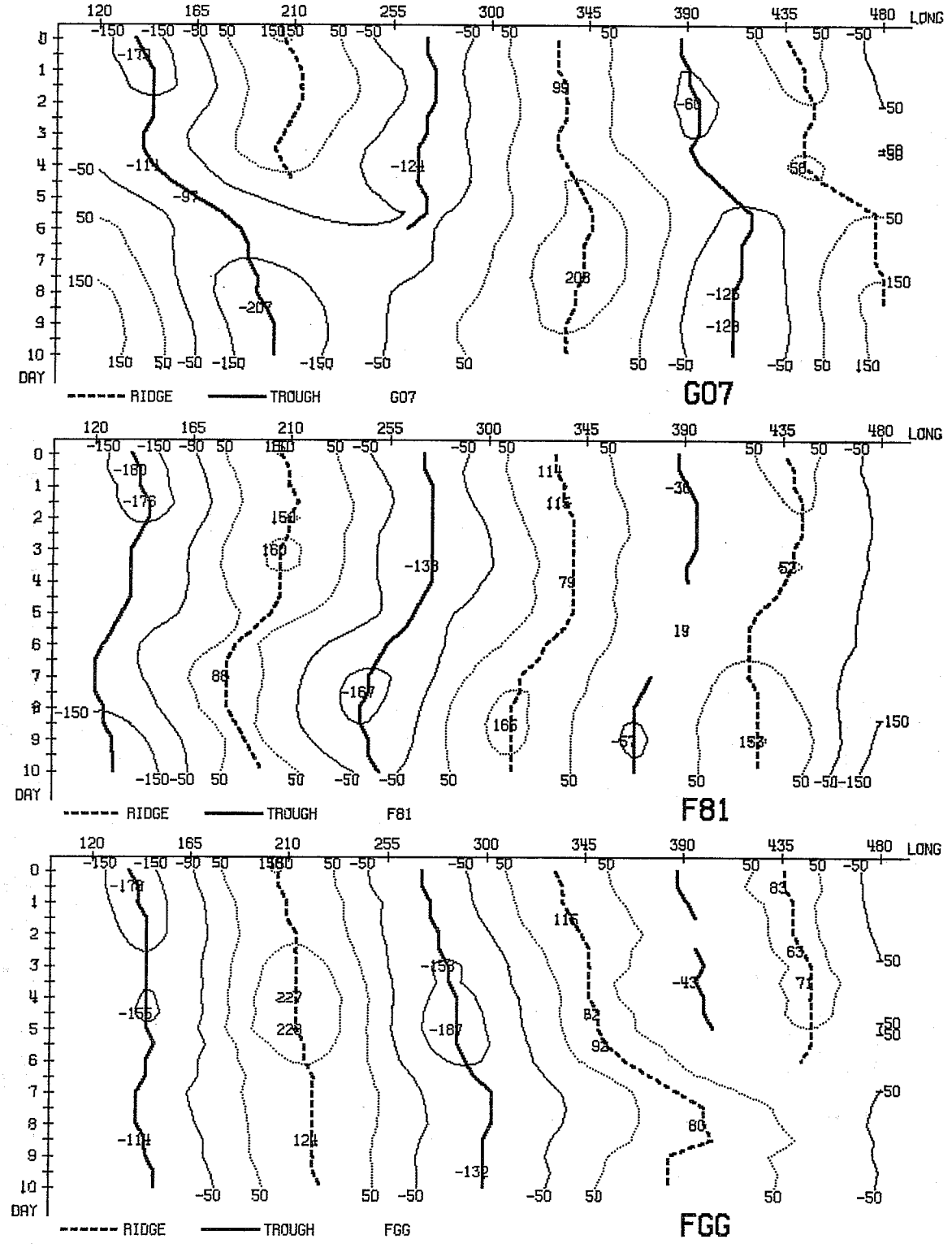


Fig. 7 Hovmöller diagrams (as Fig. 3) but for wavenumbers 1-3. G07: no mountain run. F81: control. FGG: verifying analysis.

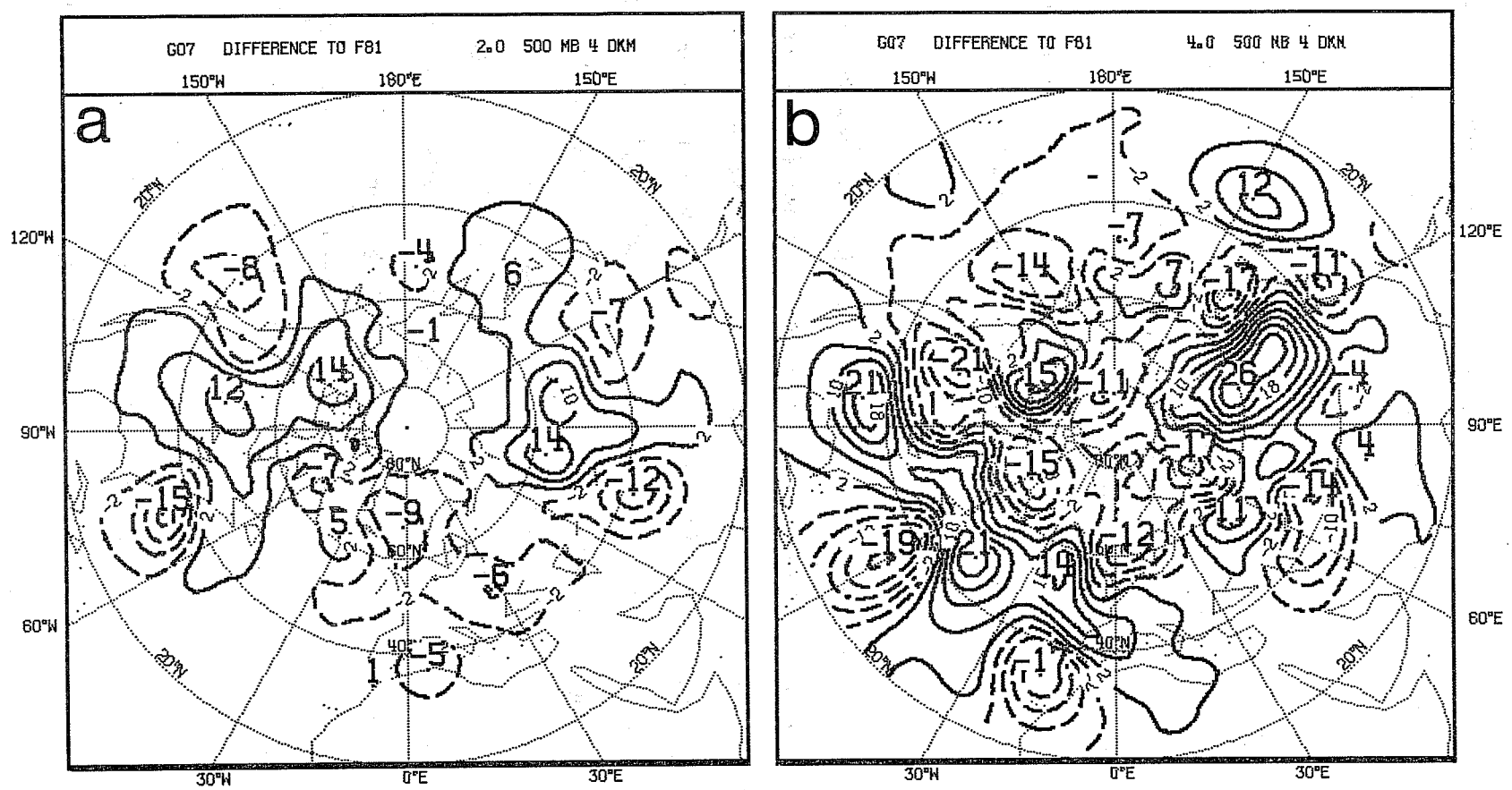


Fig. 8 Difference maps between the 500 mb geopotential heights of G07 (no mountains) and F81 (control) for day 2 (a, left) and day 4 (b, right). The contour interval is 4 dam.

Rockies can be observed in Fig.8b, consisting of a street of dipoles reminiscent of blocking high-low structures, and of split jets (see also Sect.4.3).

**4.2 The influence of the Tibetan Plateau**

It may be of interest to try to evaluate to what extent the Tibetan Plateau may influence the build-up of an Atlantic blocking. This was attempted by setting the height of the topography equal to zero within the region 15°W-180°E, 90°N-50°S (Experiment G14). It should be noted that this procedure also removes the European mountains (e.g. the Alps).

Fig.9 gives the difference maps at two day intervals between Experiment G14 and the control run. These difference maps can be interpreted as representing the propagation of the signal caused by the forcing due to the Tibetan Plateau. The major differences originate at about 75°E and propagate to reach 105°W by day 6 at an average speed of about 30° longitude per day. This corresponds approximately to the group velocity of Rossby waves for wavenumber 4 at 45°N if U=20 m/sec. At this speed the influence will propagate eastward to reach the Atlantic area in eight days. It is worth noticing the sharp transition undergone by the difference pattern across the Rockies, both in amplitude and horizontal scale. (Fig. 9c,d,e). This can only partly be explained by the progressive attenuation of the signal during its eastward propagation. Another possible reason for this is that the Rockies have an upstream (as well as downstream) influence related to their horizontal scale. Fig. 10 shows that the blocking situation is still produced in Experiment G14 although the closed high centre appears later, is weaker and slightly displaced towards the east compared with the control experiment (Fig. 3).

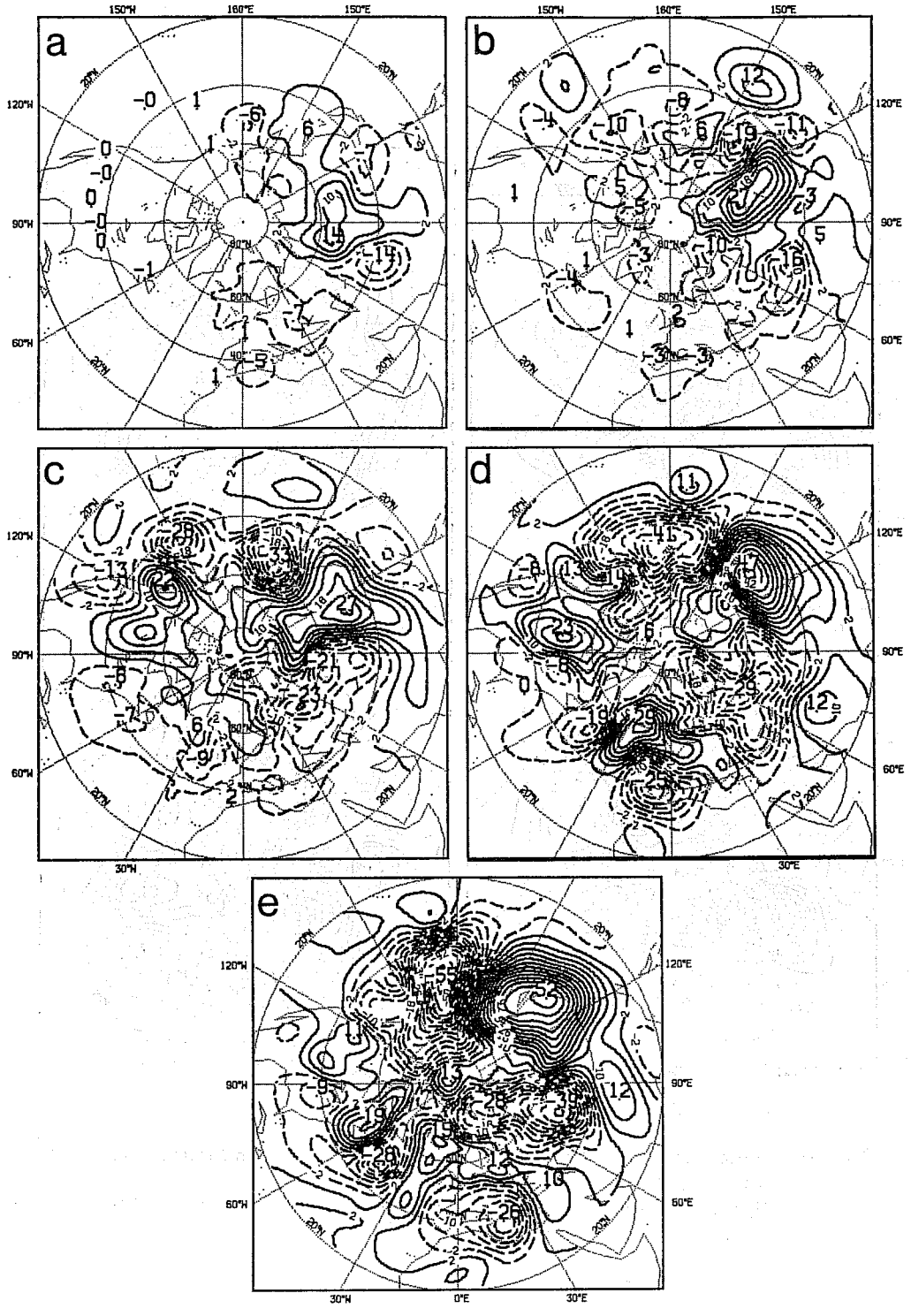


Fig. 9 Time evolution of the difference between the 500 mb height of F81 (control) and G14 (without the Tibet Plateau) for day 2 (a), day 4 (b), day 6 (c), day 8 (d) and day 10 (e).

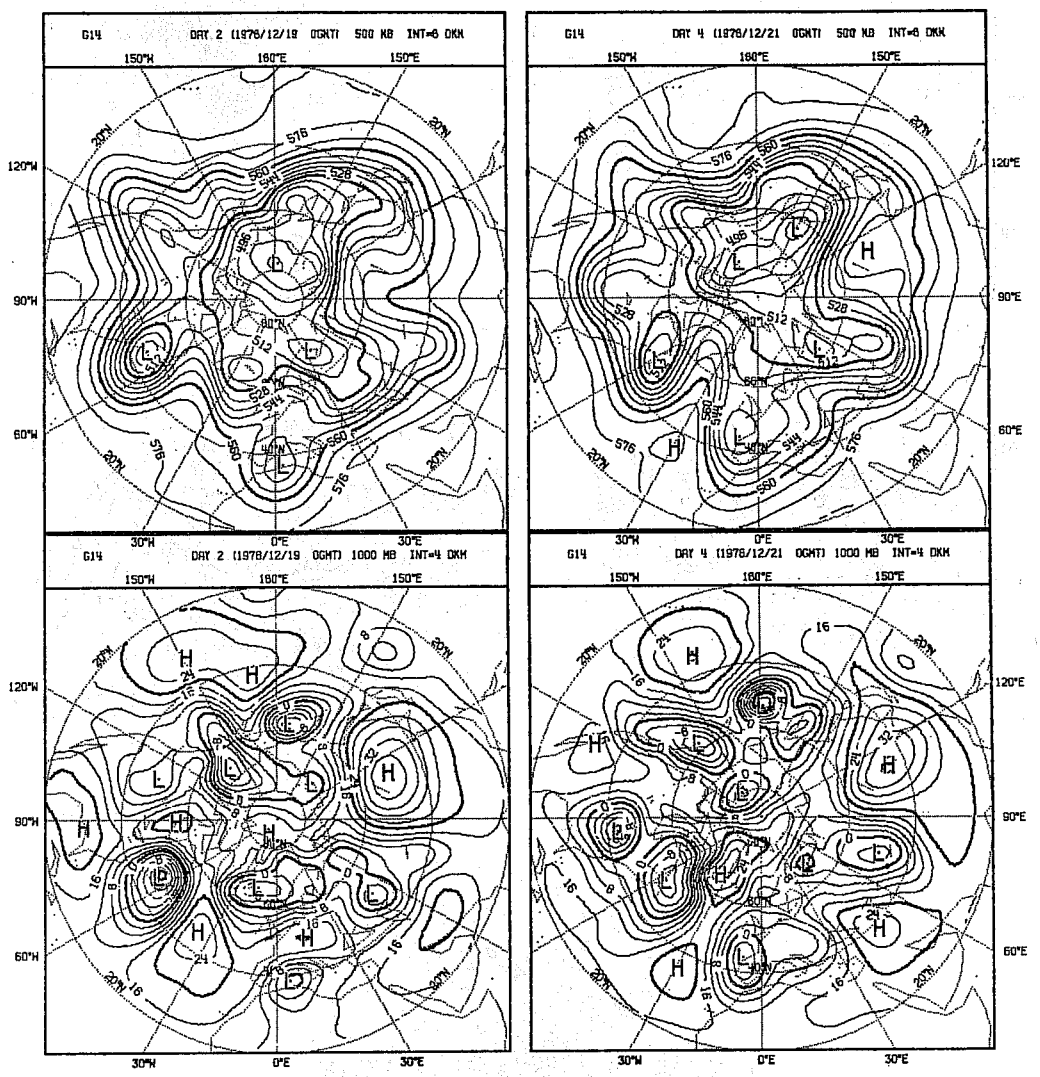


Fig. 10 Model run G14 (run without the Tibetan Plateau). (a) day 2, (b) day 4.
Upper: 500 mb height drawn every 8 dam. Lower: 1000 mb height drawn every 4 dam.

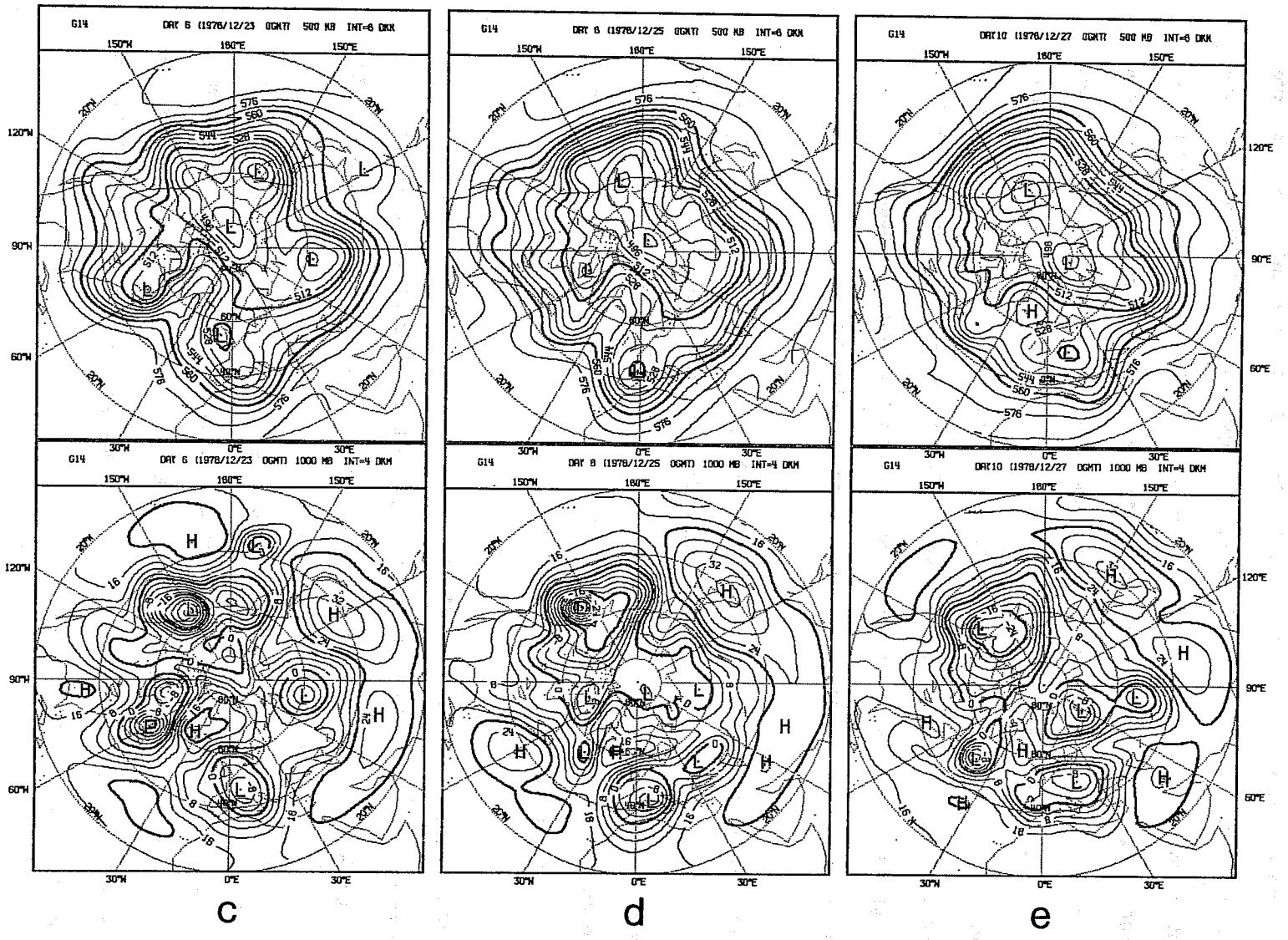


Fig. 10 (contd.) Model run G14 (run without the Tibetan Plateau). (c) day 6, (d) day 8, (e) day 10. Upper: 500 mb height drawn every 8 dam. Lower: 1000 mb height drawn every 4 dam.

### 4.3 The influence of the Rockies

Fig. 11 shows the results of Exp.G63, in which the Rockies and Greenland have been removed from the global orography. As expected, the blocking over the Atlantic never appears and is replaced by a zonal flow. As can be seen from the 500 mb height mean difference map referring to the first 5 days of the experiment, although for both forecasts the blocking has not yet been set up, the difference field already possesses features typical of a blocking pattern, i.e. an isolated high to the north and a belt of low pressure to the south, the scale being relatively small. Moreover, the 5 days mean 1000 mb height difference map presents a nearly identical pattern, suggesting the influence to be mainly barotropic in character (Fig. 12).

This result along with those described in the previous Section suggests that even a simple theoretical model of the effect of the Rockies on large-scale atmospheric motion should perhaps take into consideration its horizontal scale and the finiteness of its N-S extent. A description of such a simple analytic model is presented in Section 7.

## 5. THE EFFECT OF LAND-SEA CONTRAST

Experiment G16 was designed to isolate the effect of land-sea contrast. In order to do this, all the sea grid-points have been reset to an essentially dry soil surface condition with an appropriate value for the surface friction; the surface temperature has also initially been set equal to the lowermost air temperature value, with the intention to remove one of the main forcings the sea exerts on the atmosphere in winter time, that is the sensible heat flux. The values used for some parameters characteristic of the surface are listed in Table 1.

Fig. 13 shows that the elimination of the sea-surface from the model essentially results in the disappearance of the blocking from the forecast. The model fails to predict the splitting of the jet and the separation of the

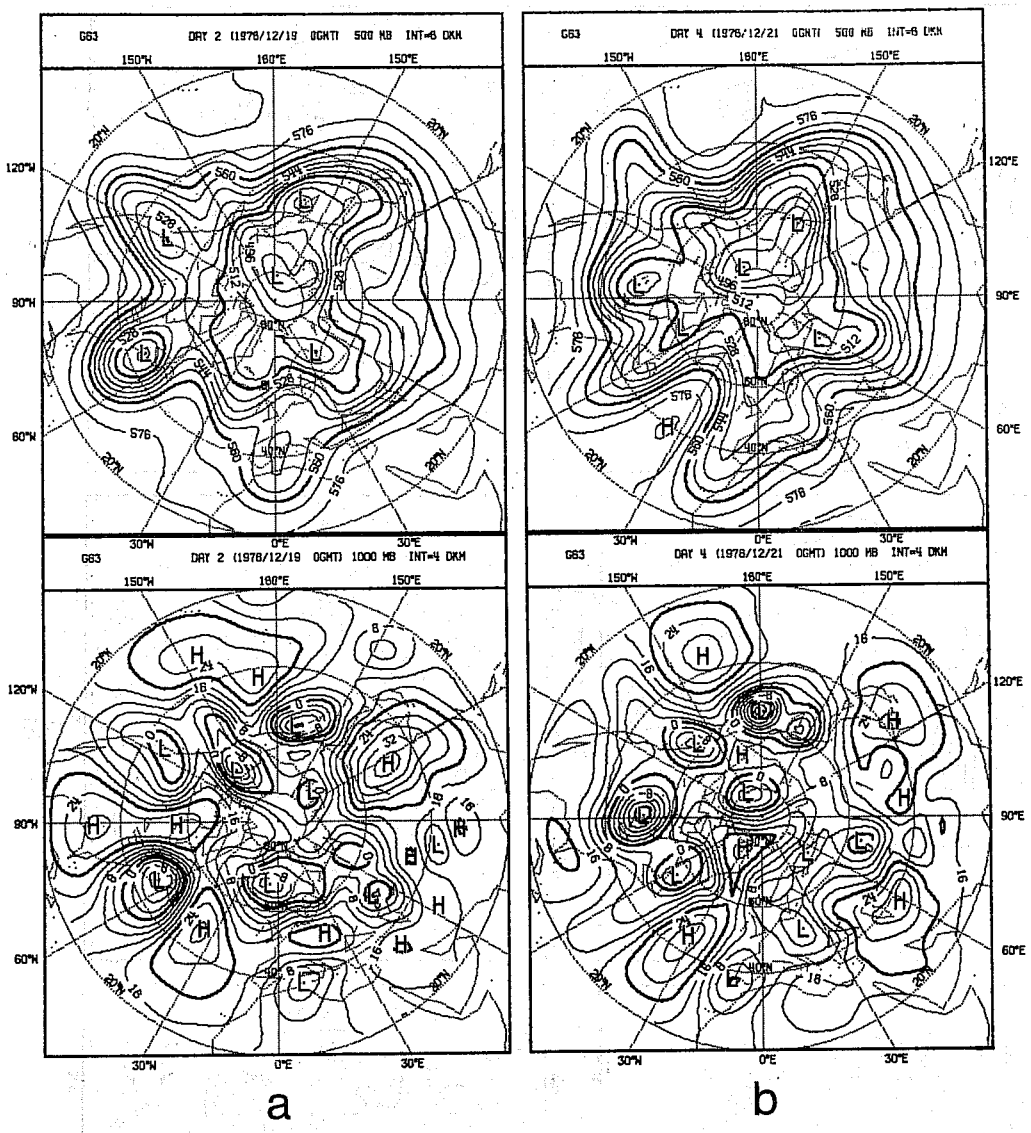


Fig. 11 Model run G63 (run without the Rockies). (a) day 2, (b) day 4.
Upper: 500 mb height drawn every 8 dam. Lower: 1000 mb height drawn every 4 dam.

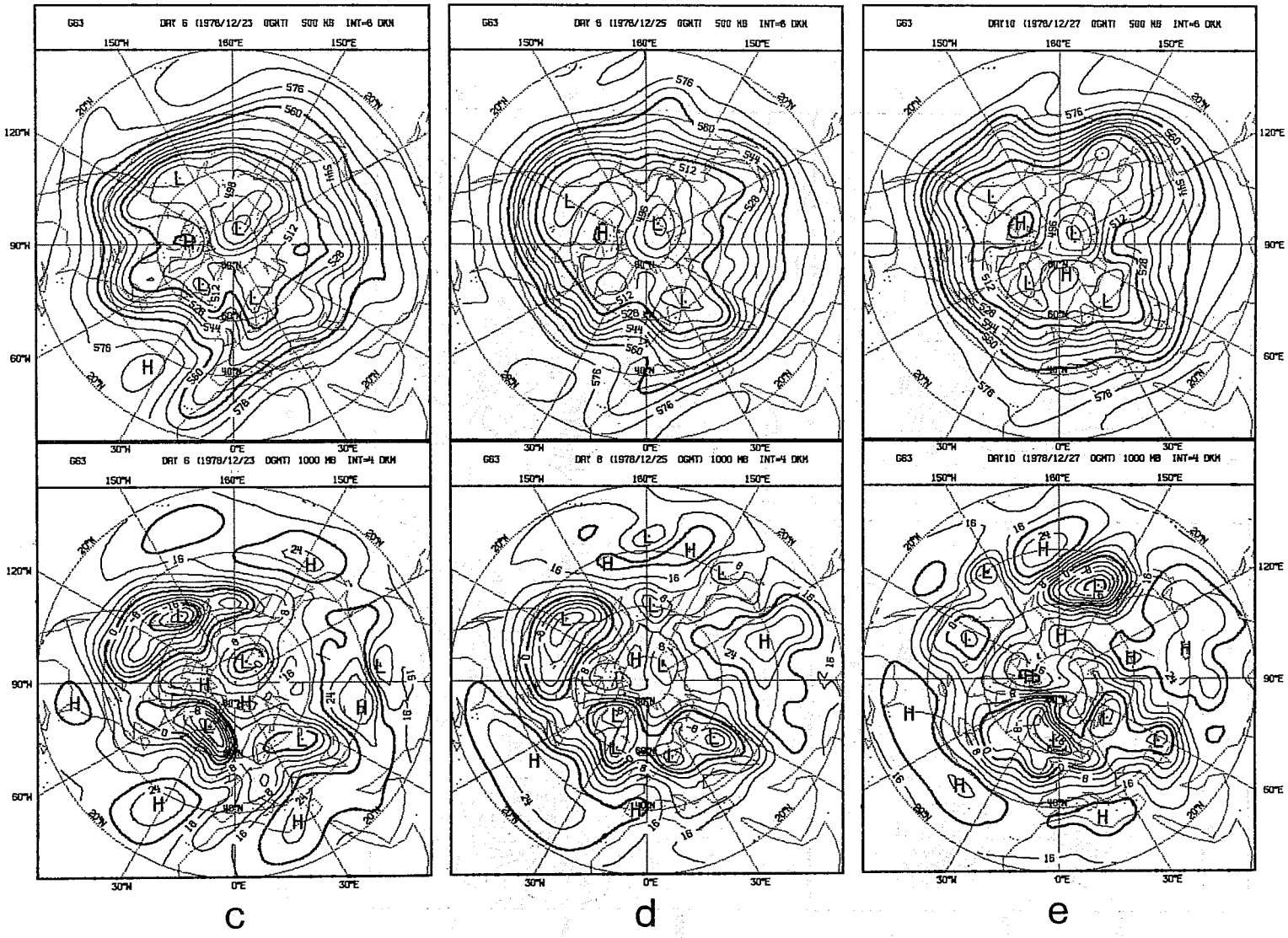


Fig. 11 (contd.) Model run G63 (run without the Rockies). (c) day 6, (d) day 8, (e) day 10. Upper: 500 mb height drawn every 8 dam. Lower: 1000 mb height drawn every 4 dam.

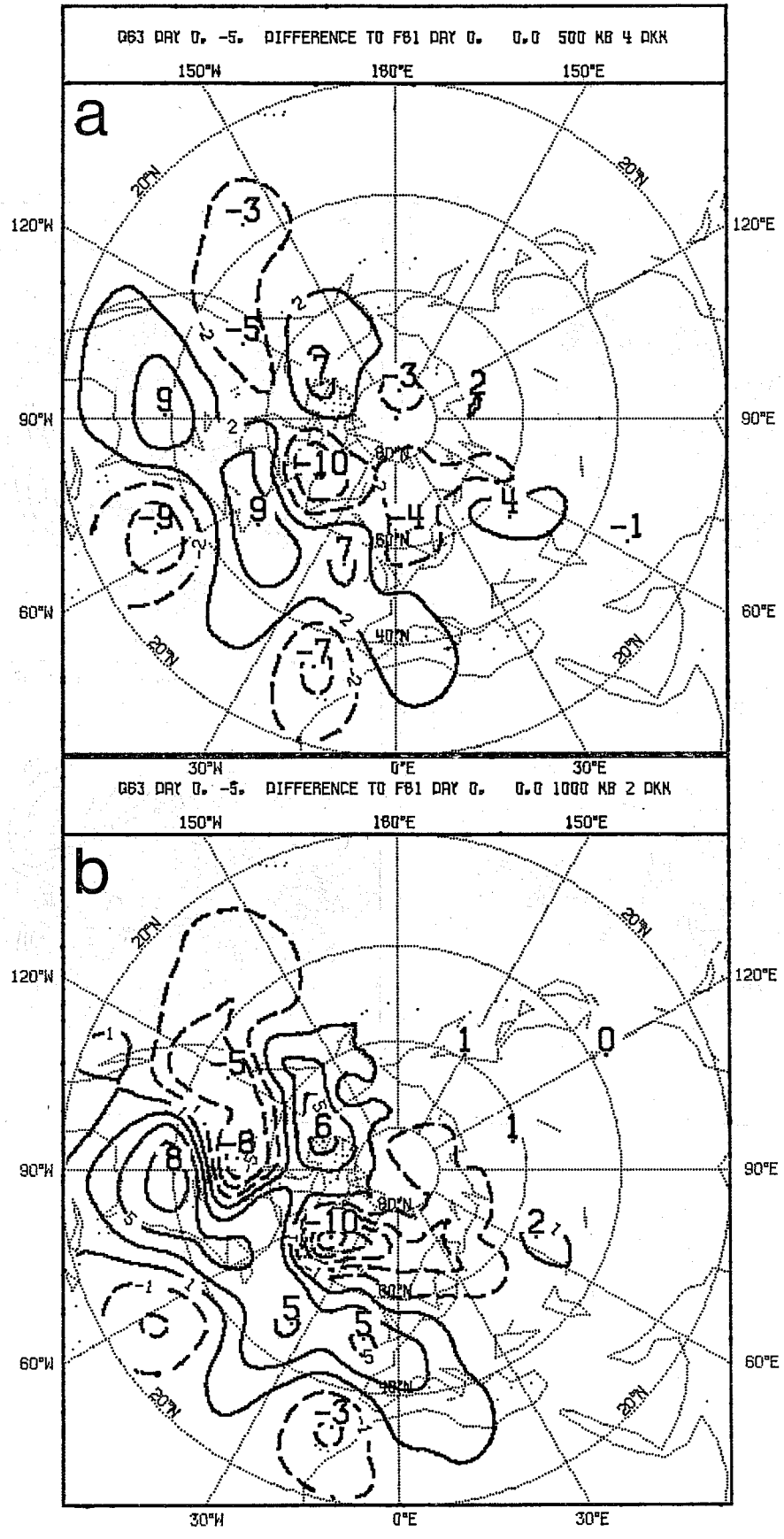


Fig. 12 Day 0 to 5 mean difference map between G63 (without the Rockies) and F81 (control). Top: 500 mb geopotential height drawn every 4 dam. Bottom: 1000 mb geopotential height drawn every 2 dam.

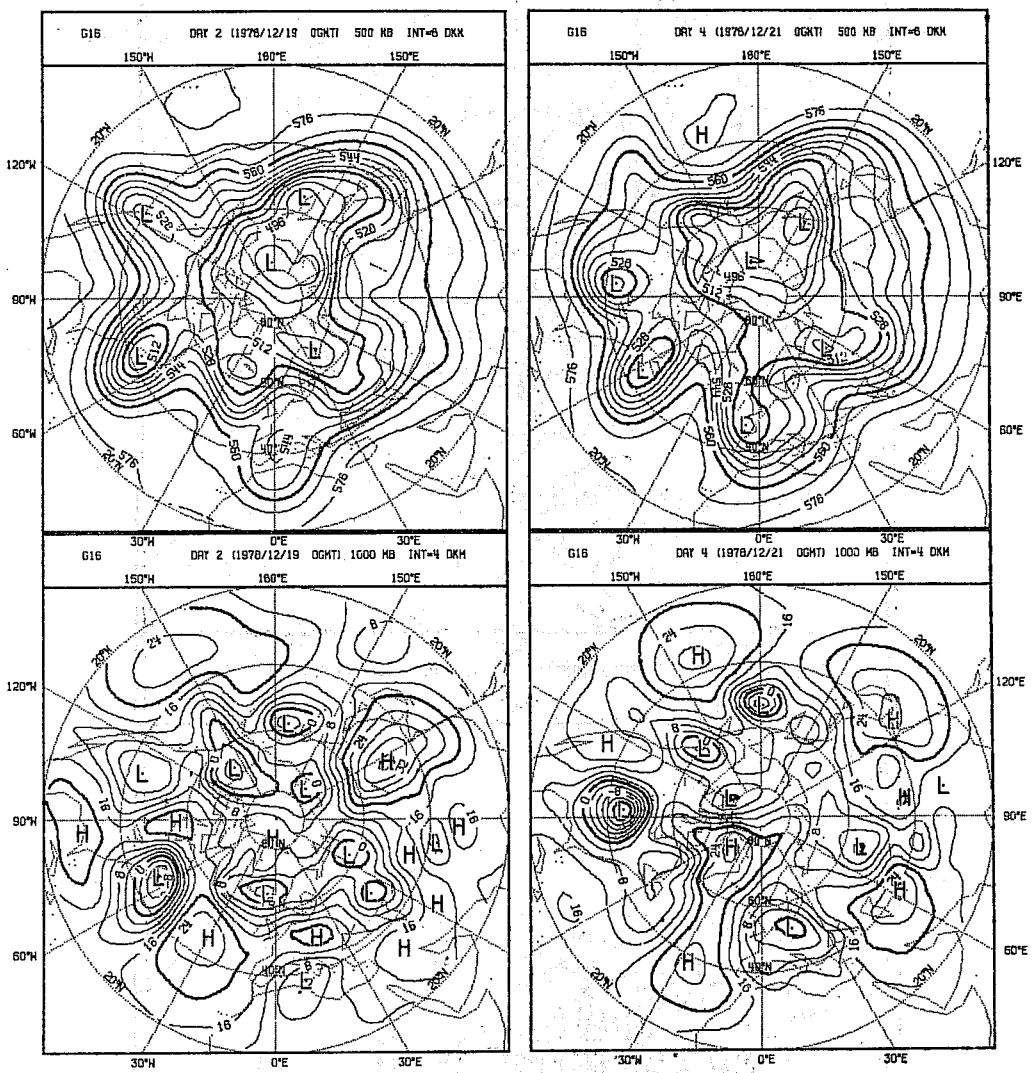


Fig. 13 Model run G16 (run without land-sea control). (a) day 2, (b) day 4.
Upper: 500 mb heights drawn every 8 dam. Lower: 1000 mb heights drawn every 4 dam.

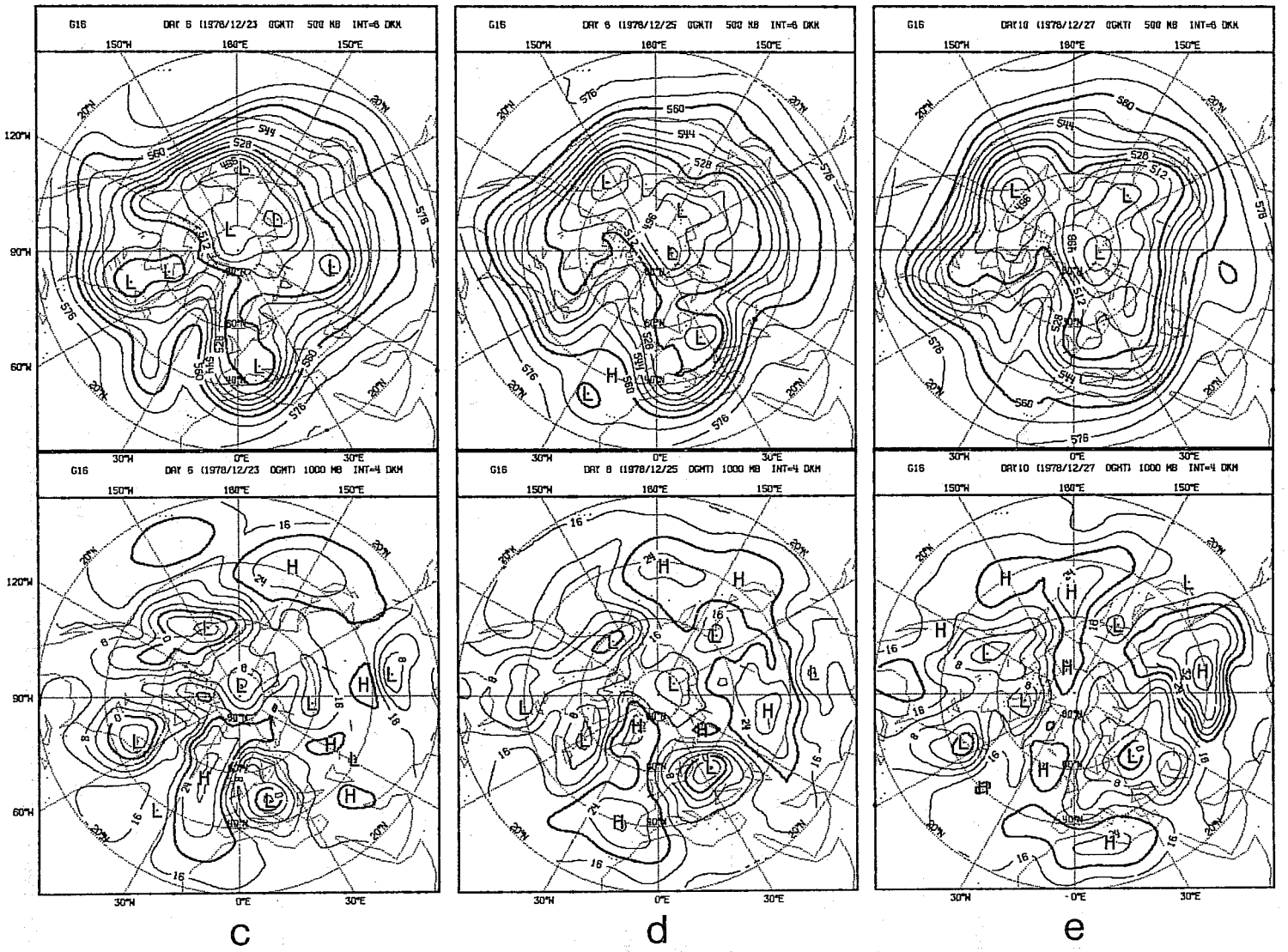


Fig. 13 (contd.) Model run G16 (run without land-sea contrast). (c) day 6, (d) day 8, (e) day 10. Upper: 500 mb height drawn every 8 dam. Lower: 1000 mb height drawn every 4 dam.

high cell, although a ridge persists over the Atlantic area throughout the later part of the 10 day forecast. This is most likely to be ascribed to the effect of the orography, as mentioned above.

Fig. 14 gives the mean difference for the first five days between experiment G16 and control. The lack of heat supply from the lower boundary and the increase of surface friction inhibit the further development of the low off the North American east coast, especially at lower levels (Fig.14b). As a consequence, the northward horizontal sensible heat flux is reduced, which is essential to the set-up of a warm high. To see this more closely, Fig.15 shows the sensible heat flux divergence and the conversion between AE (available potential energy) and KE at day 2 of the forecasts for the Atlantic area of interest. It is clear that the absence of land-sea contasts results in a reduced low-level heat supply and in a consequently reduced baroclinic activity; hence a reduction in the conversion AE-KE takes place throughout the entire troposphere.

It is also of interest to see the different distribution of precipitation over the Western Atlantic produced by the two experiments (Fig.16). For the control run, the forcing produced by the release of latent heat seems non-negligible even in winter time. The large scale precipitation alone with a maximum of 28 mm/day, is responsible for warming up the air up to about 5°C/day for the lower half of the atmosphere. Moreover, the maximum of the heating is centred at the rear of the ridge, with a phase lag of about 1/4 of wavelength, which would favour the further development of the wave and a nothward transfer of heat. For Exp.G16, the amount of precipitation is greatly reduced; in particular the amount of convective precipitation is about one half of the one produced by the control run. These differences most likely stem from the lack of moisture supply through the lower boundary and of the destabilizing effect of a warm sea surface. It might be

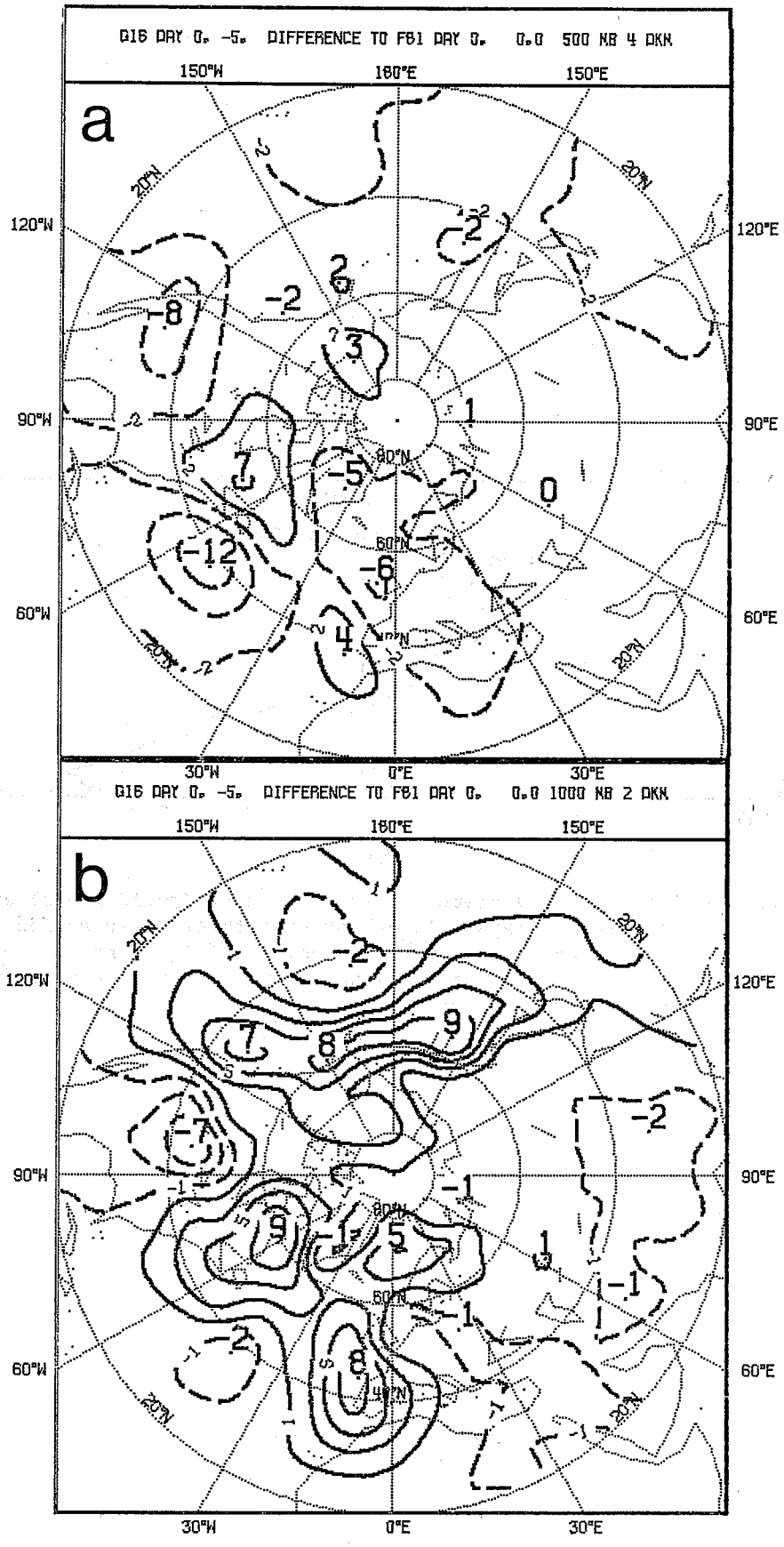


Fig. 14 Day 0 to 5 mean difference map between G16 (no land-sea contrast) and F81 (control). Top: 500 mb geopotential height drawn every 4 dam. Bottom: 1000 mb geopotential height drawn every 2 dam.

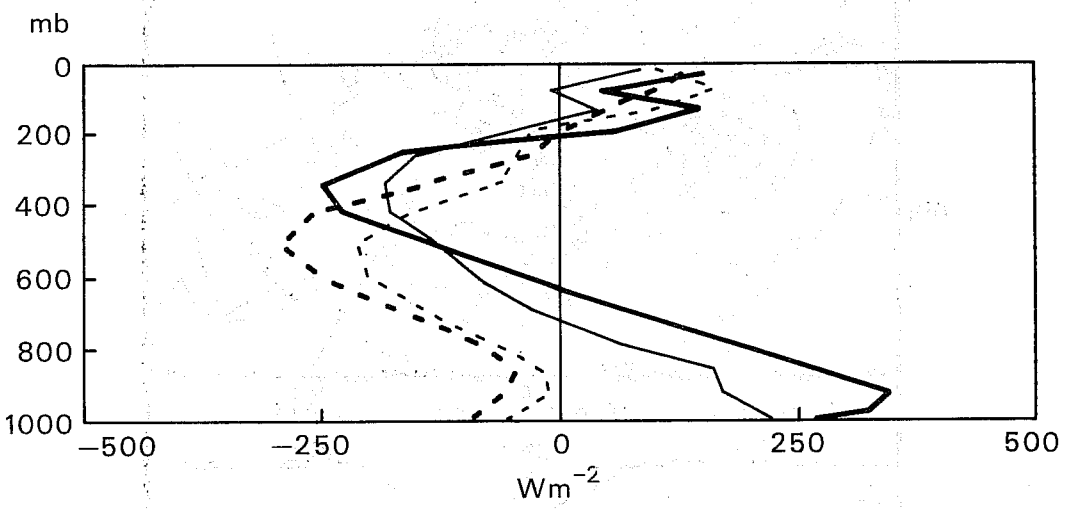


Fig. 15 Mean flux divergence of sensible heat (solid lines) and conversion (dashed lines) over North Atlantic region 30° to 70°N and 10° to 60°W for day 2. Thick lines refer to experiment F81 (control) and thin lines to experiment G16 (no land-sea contrast).

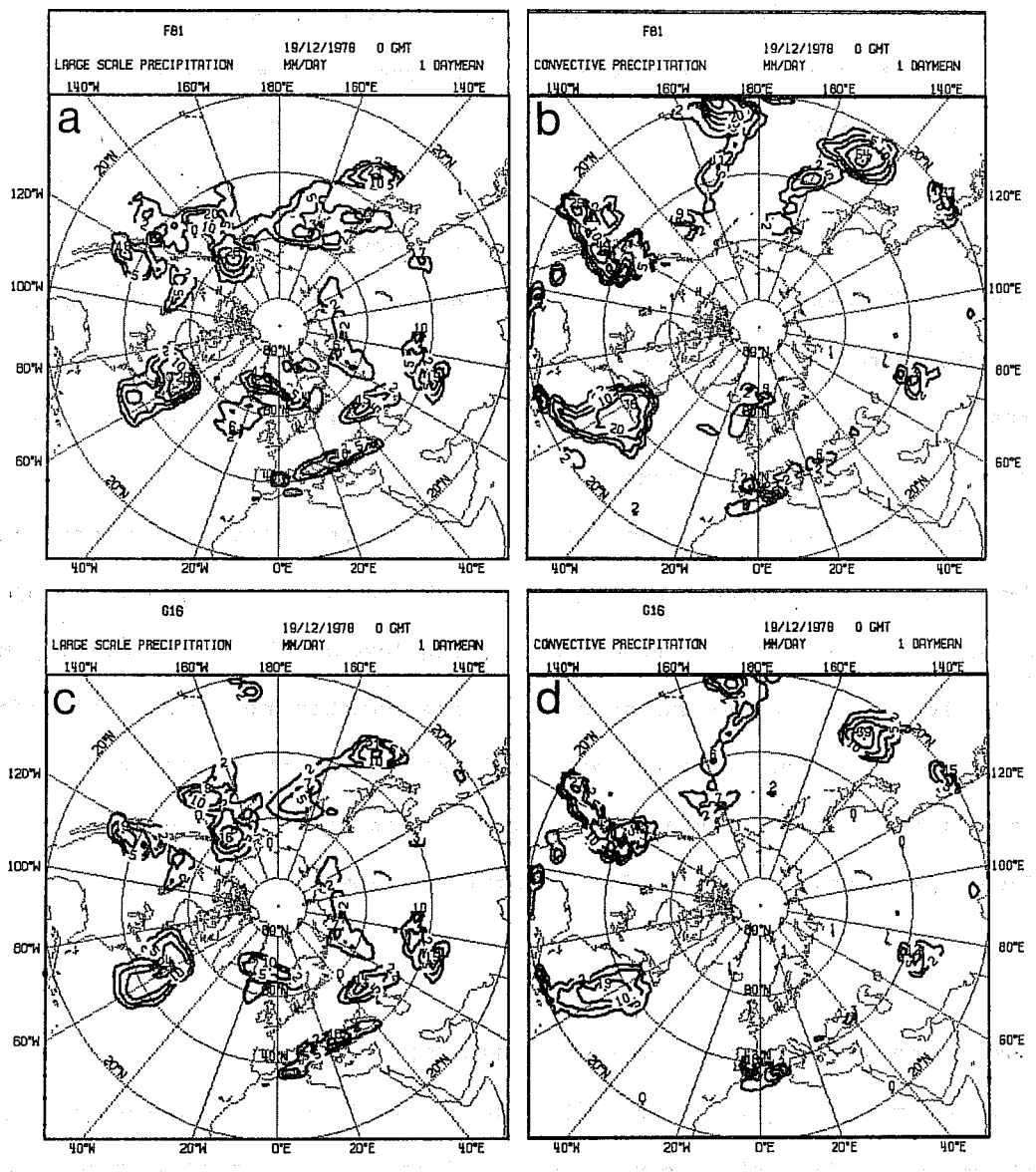


Fig. 16 Comparison of model-produced precipitation between experiment G16 (no land-sea contrast) and F81 (control) for day 2. Units: mm/day. (a) Large-scale precipitation for F81; (b) Convective precipitation for F81; (c) Large-scale precipitation for G16; (d) Convective precipitation for G16.

worthwhile to point out that the considerable heat flux, latent or sensible, coming though the sea surface (maps not shown here), is mostly confined to a limited ocean area adjacent to the east coast of North America and seems to be more a phenomenon taking place on the long wave scale than on the ultra-long wave scale.

This result, together with those mentioned in Sect. 4.1, suggest that the influence of land-sea contrast evidences itself in enhancing the intensity of the development of the low near the coast thus reinforcing the effect of orography, even for a climatological sea surface temperature (SST) distribution. It can, therefore, be generally of importance, as it is in this particular case, for the onset of a blocking event. However, the land-sea contrast alone does not seem to be the forcing chiefly responsible for controlling the positioning of the ensuing large-scale trough development and its locking in phase so crucial to the maintenance of the blocking pattern. We therefore conclude that, at least in this particular case study and as far as the maintenance of the block is concerned, the effect of the land-sea contrast is of secondary importance compared to the orographic effect.

## 6. THE INFLUENCE OF DIABATIC EFFECTS (THE MODEL "PHYSICS")

Exp.F98 and Exp.I14 were designed with the aim to identify the overall effect of the model's "physics", including sub-grid scale energy sources and sinks. Both runs are esentially adiabatic and only a small surface friction (corresponding to a sea-type surface) is included; I14 has mountains, while F98 has not.

First of all, as can be seen from Table 1 the no-mountain minimum physics run shows the worst objective scores of all experiments. This confirms the conclusion arrived at by Bengtsson (1981) that in order to obtain useful predictability of blocking on a time scale greater than 5 days, high

resolution and realistic model physics are both of importance.

Secondly, both Fig. 17 (F98) and Fig. 18 (I14) show model runs mainly characterised by overdevelopment of systems, leading to an excessive growth of eddy KE. This suggests that we have removed more energy dissipating factors than energy supplying factors. It is interesting that, although in experiment F98 the overdevelopment taking place over the East Coast of North America does bring about a rapid onset of a blocking feature on day 7, this dies away right after one day. As can be seen from the Hövmoller diagram (Fig. 7), no successive troughs are observed within the region between 90°W and 60°W. This is obviously different from the control run F81 and again illustrates the dominating effect of orography on the maintenance of blocking. Conversely, the minimum physics experiment with mountains (I14) produces the setup and maintenance of the block, to some extent, although it is affected by an obvious misrepresentation of the behaviour of the northern branch of the jet (see Fig. 18b,c). Since in Exp.I14 the land-sea contrast has of necessity been eliminated together with most other diabatic effects, it comes natural to compare it with experiment G16(Fig. 13) that similarly had mountains and no land-sea contrast, but also had all model's physics (vertical turbulent diffusion, condensation effects, clouds and radiation). The results of this comparison are somewhat puzzling, since it would seem that the introduction of these diabatic efffects in the modelling has the net effect of deteriorating even further the maintenance of the 'blocking', contrary to what one would, a priori, expect. This apparent inconsistency can, however, be reconciled thinking in terms of the life cycle of the East Coast development crucial to the onset of the Atlantic Block. Removing the sea-located heat sources but leaving the diabatic effects of moisture condensation (Exp.G16) results in a shortening of the life of this perturbation, in a consequently reduced overall baroclinic efficiency of the high-low system and therefore in a very weak blocking ridge. If, however,

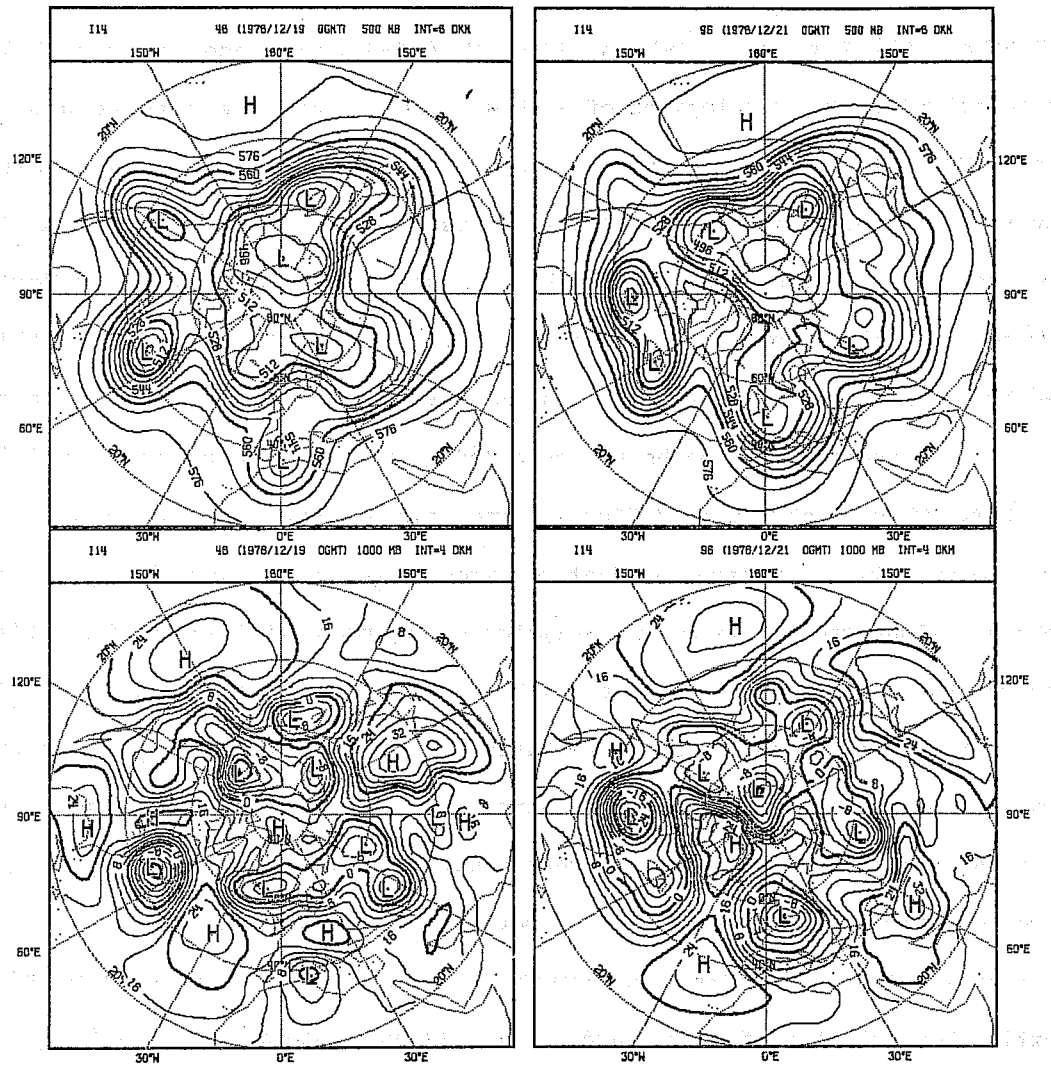


Fig. 17 Same as Fig. 2 but for experiment F98 (adiabatic, no mountains). a) day 2, b) day 4.
Upper: 500 mb height drawn every 8 dam. Lower: 1000 mb height drawn every 4 dam.

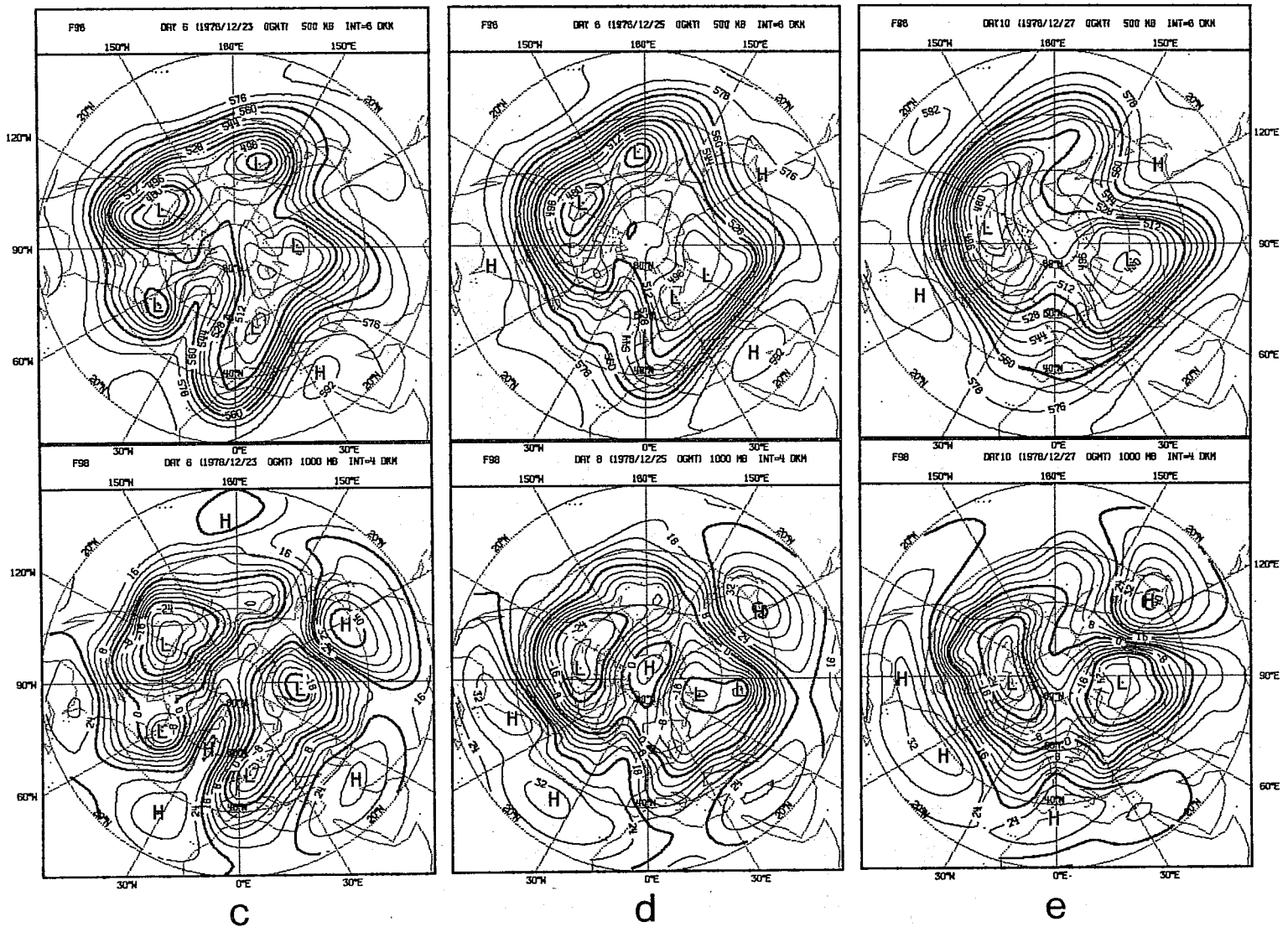


Fig. 17 (contd.) Same as Fig. 2 but for experiment F98 (adiabatic, no mountains). c) day 6, d) day 8, e) day 10. Upper: 500 mb height drawn every 8 dam. Lower: 1000 mb height drawn every 4 dam.

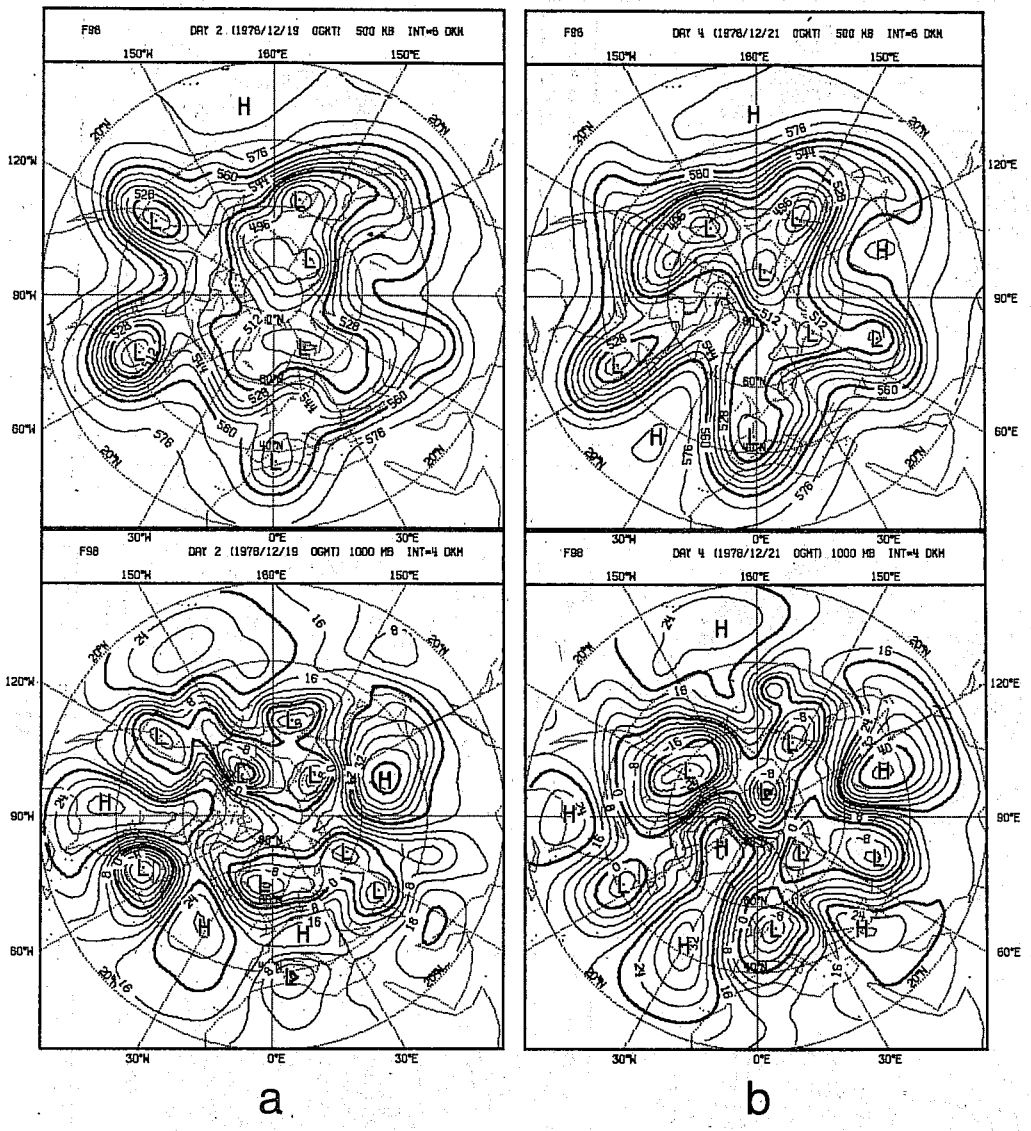


Fig. 18 Same as Fig. 2 but for experiment I14 (adiabatic, with mountains). a) day 2, b) day 4.
Upper: 500 mb height drawn every 8 dam. Lower: 1000 mb height drawn every 4 dam.

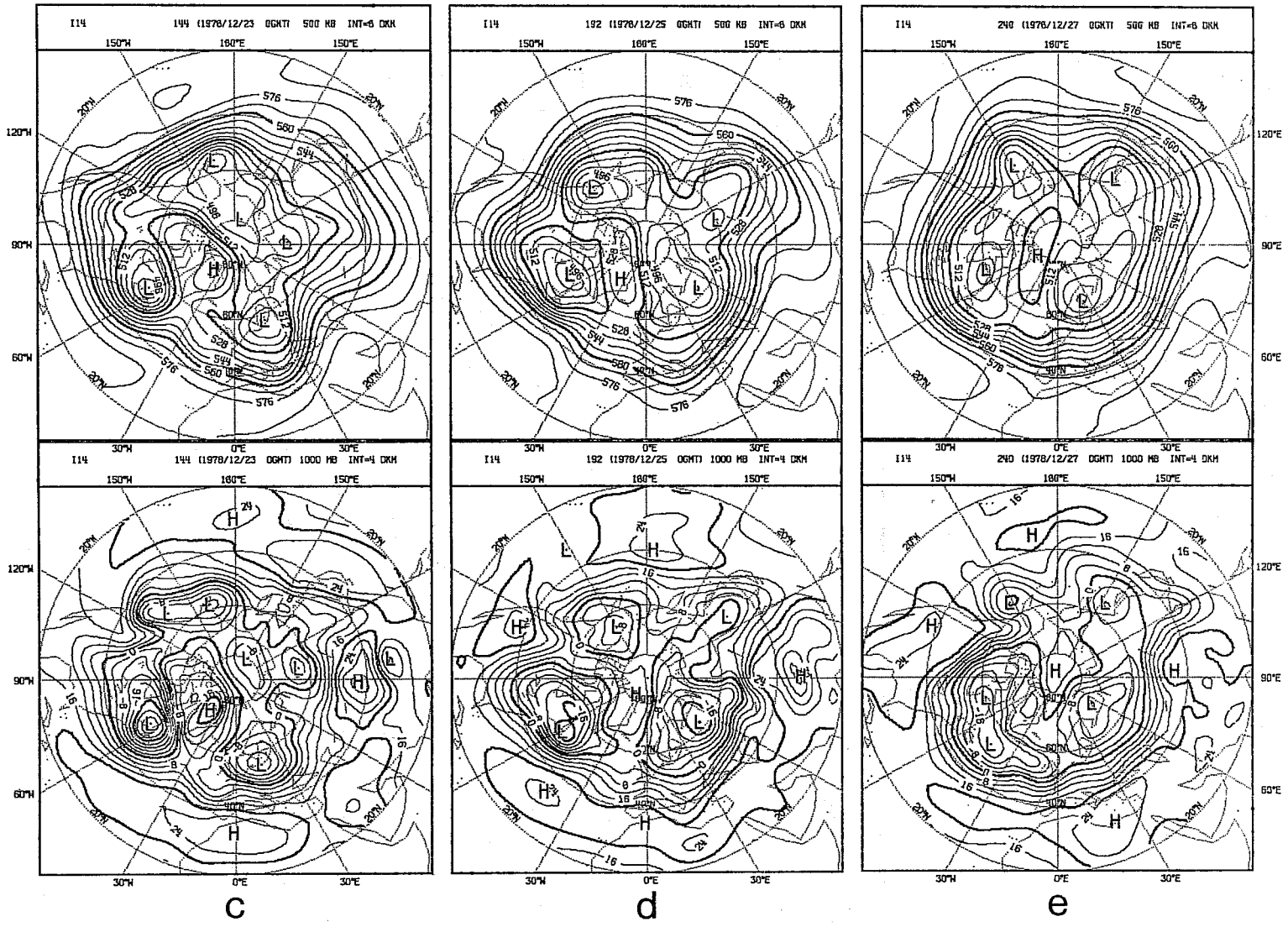


Fig. 18 (contd.) Same as Fig. 2 but for experiment I14 (adiabatic, with mountains). c) day 6, d) day 8, e) day 10. Upper: 500 mb height drawn every 8 dam. Lower: 1000 mb height drawn every 4 dam.

the absence of the surface heat source is overlapped with the absence of condensation effects, the quasi-adiabatic development of the low regains strength and is able to prepare the right conditions for the onset of the blocking ridge. It is also interesting to note at this stage that I14 is the experiment that best captures the longitudinal phase positioning of the blocking doublet, better even, in this respect only, than the control experiment, heavily affected by an eastward displacement of the blocking feature.

## 7. A SIMPLE ANALYTIC MODEL OF THE INFLUENCE OF THE ROCKIES ON LARGE SCALE FLOW

As mentioned in Section 4.3, the difference fields for 1000 mb geopotential (and, to a slightly lesser extent for 500 mb geopotential) between control and the no-Rockies experiment show a regional feature characterized by two strips of alternatively inverted dipoles, stretching to the east of the (missing) Rockies. The first dipole (longitude of the axis around 90W, see Fig. 12a) has the negative maximum of 8 dam at 50°-55° N and the positive maximum, again of 8 dam, around 40° N. The second dipole, much weaker in intensity, is centered around 60° W with positive maximum to the north and negative maximum to the south. The third dipole (positive maximum to the south and negative to the north) lies around 40° W and the fourth around 15°W. This signature seems to be connected with the meridional variation of the mountain profile, this being particularly important to the Rockies, comparatively narrow in the E-W direction but largely elongated along the N-S.

Malguzzi and Speranza (1981), discussing the possibility of obtaining block like solutions as a product of local multiple-equilibria, take into account non-sinusoidal orography and obtain flow patterns reminiscent of a street of

dipoles (cf.their Figs. 5 and 8). In this Section we attempt a very simple analytical interpretation, using an equivalent-barotropic atmosphere, of the effect of a mountain with a finite N-S extent on a train of large-scale propagating planetary waves.

Starting from the well-known vorticity ($\zeta$) equation in p-coordinates:

$$\frac{\partial \zeta}{\partial t} + \underline{V} \cdot \nabla (\zeta+f) = f_o \frac{\partial \omega}{\partial p} \tag{1}$$

with linearized boundary conditions

$$\omega = 0 \qquad \text{at } p = o \tag{2a}$$

$$\omega = -\rho_o \, g \, \underline{V}_o \cdot \nabla z_* \qquad \text{at } p = p_o \tag{2b}$$

where $z_*$ is the height of the orography, $p_o$ is the surface pressure (taken as a constant, hence the linearizations of the boundary conditions) and all other symbols are used in their common meaning. Vertical advection of vorticity and twisting terms have been neglected in (1) following, e.g., Lorenz (1960).

Integrating (1) in the vertical for an equivalent barotropic atmosphere under conditions (2) gives:

$$\frac{\partial \tilde{\zeta}}{\partial t} + \tilde{\underline{V}} \cdot \nabla (\tilde{\zeta}+f+h_*) = 0 \tag{3}$$

where $h_* = f_o \, \alpha \frac{z_*}{H}$, $H = \frac{RT_o}{g}$ (scale height) and

$\alpha$ is a constant proportional to the ratio $|\underline{V}_o|/|\tilde{\underline{V}}|$.

Eqn.(3) now applies to an "equivalent barotropic" level (the symbol ~ indicating quantities at this level) and subscript o indicates quantities evaluated at the lower boundary.

If we now linearize (3) with respect to a purely zonal flow $\bar{u}$, we obtain:

$$\frac{\partial \zeta'}{\partial t} + \bar{u} \frac{\partial}{\partial x} (\zeta' + h_*) + \beta v' = 0 \qquad (4)$$

where $\zeta'$ and $v'$ now indicate perturbation quantities and $\bar{u}$ can still be considered a function of y (and in this case $\beta = \frac{\partial f}{\partial y} - \frac{\partial^2 \bar{u}}{\partial y^2}$). Since we are only interested in a "regional" effect in the immediate lee of the mountain and for simplicity, we will neglect the $\beta$ term in (4): this is equivalent to consider that the typical E-W wavenumber of the mountain is $\gg (\frac{\beta}{\bar{u}})^{\frac{1}{2}}$, that is the mountain has a narrow E-W scale.

Now assume $h_*$ and hence $\zeta'$ to be of the form

$$\zeta' = \mathrm{Re} \left[ A_\zeta(y,t) \exp \left( i [kx - \delta_\zeta(y,t)] \right) \right] \qquad (5a)$$

$$h_* = \mathrm{Re} \left[ A_*(y) \exp \left( i [ kx - \delta_*(y)] \right) \right] \qquad (5b)$$

where $A_\zeta$ and $\delta_\zeta$ are real quantities. This is equivalent to choosing a perturbation plane wavetrain moving over a cosine-profile topography of the same wavelength along x. Substituting (5) in (4) and solving for real and imaginary part separately gives:

$$\frac{\partial A_\zeta}{\partial t} = A_* \bar{u} k \sin (\delta_\zeta - \delta_*) \qquad (6a)$$

$$\frac{\partial \delta_\zeta}{\partial t} = k\bar{u} + \frac{A_*}{A_\zeta} \bar{u} k \cos (\delta_\zeta - \delta_*) \qquad (6b)$$

Equations (6) describe the local rate of change of, respectively, the wave amplitude and phase (Chen, 1980). An intuitive consequence of Eqn.6a is that, when a trough is moving in the region in the lee of the mountain ($\delta_\zeta - \delta_* \in [\ 0, \pi\ ]$), it also develops, since its amplitude is increasing in time. Equations (6) also tell us that we may expect a variation of the local

phase speed of the wave ($\partial\delta_\zeta/\partial t$) with latitude (y-coordinate) due to the north-south variations of the mountain profile. If we then imagine a train of large-scale waves approaching a mountain with a finite north-south extent, we can expect variations in the local phase speed that will produce local retardation (or acceleration) of the approaching wave and therefore, tilting of the otherwise north-south oriented trough (and ridge) axes.

If we now try to estimate what the effect of such tilting on the north-south eddy momentum transport associated with the propagating waves would be, we can infer if and where (along y) the effect of the mountain is to slow down or to accelerate the mean westerlies.

Considering the wave problem sketched above in terms of a perturbation streamfunction $\psi'$ expressed in the same form as (5), the geostrophic eddy momentum flux within one wavelength $L_x$ can be expressed as:

$$\overline{u'v'} = \frac{1}{L_x}\int_0^{L_x} -\frac{\partial\psi'}{\partial x}\,\frac{\partial\psi'}{\partial y}\,dx = \frac{k}{2}A_\psi^2\,\frac{\partial\delta_\zeta}{\partial y} \qquad (7)$$

where $A_\psi$ is the amplitude of the perturbation streamfunction $\psi'$ and the meridional variation of the streamfunction phase $\frac{\partial\delta_\psi}{\partial y}$ has been replaced by $\frac{\partial\delta_\zeta}{\partial y}$, implying consequently that streamfunction and vorticity should show the same tilting of the north-south trough-ridge axes. This is immediately evident in the case of a perturbation periodic in y (with wavenumber $\ell$) because in such a case it would be $\zeta = \nabla^2\psi$ and $\partial_{yy}\psi = -\ell^2\psi$.

Making use of (6b), (7) can be rewritten

$$\frac{\partial}{\partial t}\,\overline{u'v'} = \frac{k^2}{2}\,\bar{u}\,A_\psi^2\,\frac{\partial}{\partial y}\left[\frac{A_*}{A_\zeta}\cos\,(\delta_\zeta-\delta_*)\right] \qquad (8)$$

where, again for simplicity, we have used the assumption that the basic state

has no latitudinal variations.

The intuitive meaning of (8) is now very clear; it indicates that the local rate of change of momentum flux is determined by the north-south slope of the mountain and by the phase relationship between the mountain and the waves and is proportional to the mean flow speed $\bar{u}$ and to the amplitude of the perturbation streamfunction $A_\psi$.

If we choose to fix our attention on the effects of the meridional variation of the mountain slope and to the instant in which the topographically reinforced trough is in the lee $(\delta_\zeta - \delta_* \in [\frac{\pi}{2}, \pi]$, hence $\cos(\delta_\zeta - \delta_*) < 0)$, we see that

$$\frac{\partial A_*}{\partial y} < 0 \quad \text{implies} \quad \frac{\partial}{\partial t}\,\overline{u'v'} > 0$$

like, for example, at the northern end of the north-south extending chain, and

$$\frac{\partial A_*}{\partial y} > 0 \quad \text{implies} \quad \frac{\partial}{\partial t}\,\overline{u'v'} < 0$$

at its southern end.

The net result is increase of horizontal westerly momentum at both ends of the mountain and decrease in the middle; this means that the net effect of this transient behaviour is to slow down the westerlies in the central part of the region immediately in the lee of the mountain and to accelerate them at both north and south ends of it. This would tend to produce a "trailing" trough north of the barrier (eastward tilt with latitude) and a "leading" trough south of it, see Fig. 19. This can be interpreted as a tendency to "split" the westerly jet into two separate branches, favouring, in this way,

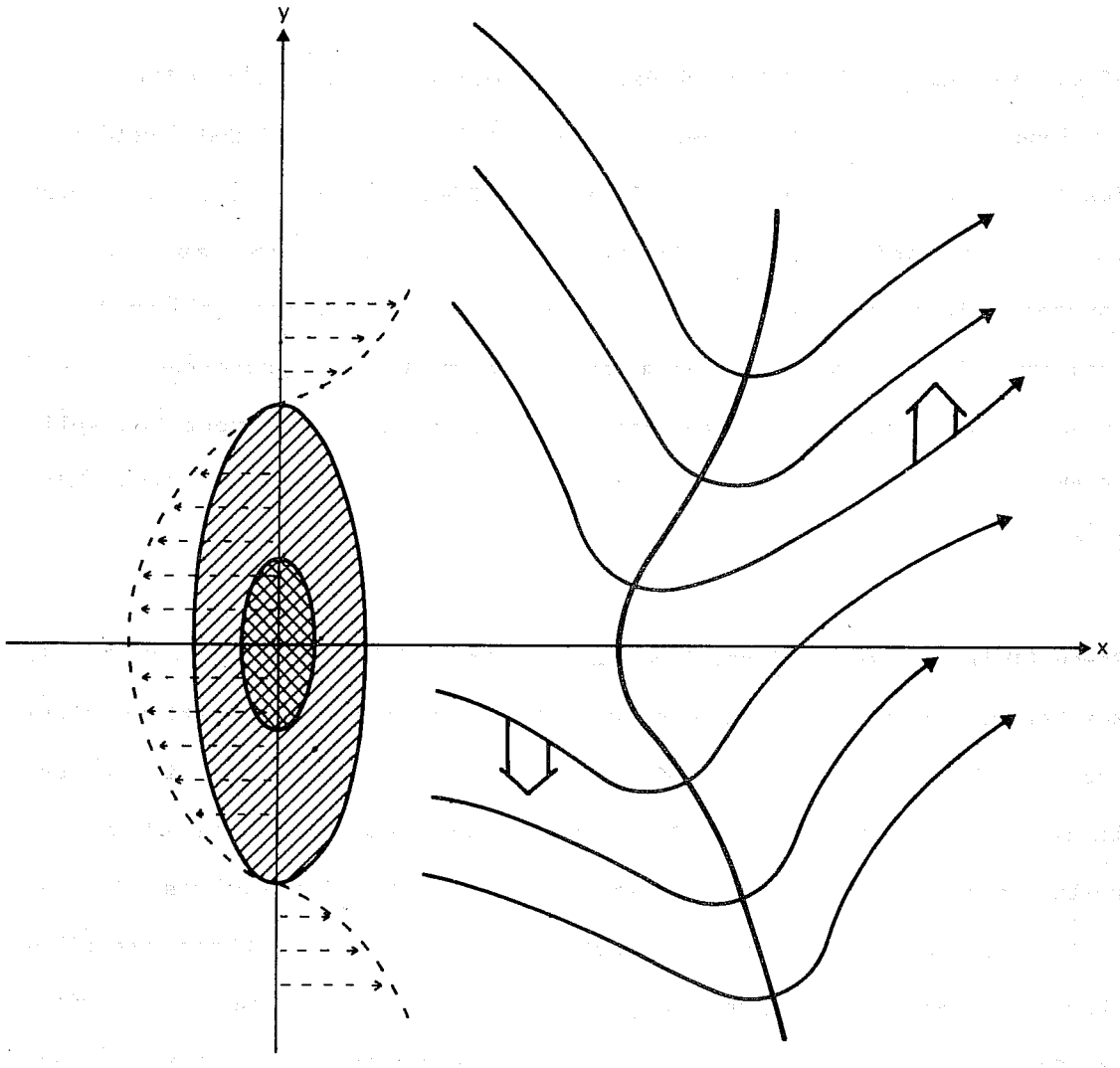


Fig. 19 A schematic diagram describing the tilting of an eastward-propagating large-scale trough in the lee of a North-South elongated mountain. Thin solid lines : stream lines. Thick solid line : trough axis. Large arrows show the direction of westerly momentum transfer and thin dashed arrows, the change in the zonal flow.

both onset and maintenance of a blocking pattern.

Of course, given the E-W periodicity of our analysis, the effect now mentioned would integrate to zero if integrated over one full E-W wavelength, due to the compensating (jet-splitting) effect of the mountain-trough interaction and of the (jet-rejoining) effect of the succeeding mountain-ridge interaction. If, however, the oncoming wavetrain is evanescent (or has evolved) in time in such a way to give preference to the trough rather than to the ridge, the net effect will be to favour the split of the westerly jet in the lee of the barrier (e.g. Kalnay-Rivas and Merkine (1981)).

Green (1977) has stressed the importance of the eddy transfer of momentum in maintaining the blocking anticyclone. These simple considerations might provide a link with the effect of orography. It is also interesting to see in the work by Malguzzi and Speranza, (1981) that the insertion of a realistic orography in their analytical channel-type model produces a stable equilibrium state that shows wave patterns very similar to those described above and compatible with our interpretation of Eqn.8 (see Fig. 8 in Malguzzi and Speranza, 1981). The idealized numerical experiments by Kalnay-Rivas and Merkine (1981) with a Rockies-like obstacle in a wavy zonal flow also show similar features.

## 8. CONCLUDING REMARKS

There are several objections that can be made to this type of numerical experiments. For instance, the conclusions that can be drawn by a simple case study have limited applicability and the level of complication of the numerical model used is such that all its components are highly interactive in a deeply non-linear fashion. On the other hand, we feel that the

existence of GCM-type models that are able to reproduce real blocking cases, at least to a point, should be exploited to try to bridge the gap between highly simplified models and real data diagnostic studies.

Having in mind the limitations of the present investigation, the following conclusions can be derived:

a) For a blocking to become established an intense development seems necessary; this coincides with an increase in the wavenumber 4 to 9 kinetic energy and therefore stresses the direct importance of the representation of synoptic-scale waves in numerical models. It should, however, be remembered that the importance of the synoptic scales for maintenance of blocking can also be felt via the (non-linear) interactions that these shorter scales can have with longer planetary-type waves; see also Tibaldi and Ji (1982).

(b) The effect of the earth's orography seems essential for both the build-up and the maintenance of the blocking pattern, but in particular for its maintenance. The role of the orography in controlling successive in-phase interactions between transient eddies and standing waves (and particularly in the maintenance of the latter) seems to be paramount.

(c) A degree of "locality" can be recognized in the role of large-scale orography. This is to say that the effect of removing part of the orographic forcing (e.g. in a particular geographical location) has the effect of generating a train of spuriously (mainly eastward) propagating Rossby-type waves that would otherwise be locked in phase. If the area of concern is to the east and nearer to the orographic feature "removed", the disrupting effect is immediate. On the other hand, within 8 to 10 days the whole hemisphere will be severely affected.

(d) The influence of land-sea contrast on blocking seems to be mostly confined to controlling the intensity of the intense development that initiates the process, reinforcing the effects of the orography and of the intrinsic wave baroclinity. Its importance seems to be limited to the build-up of the blocking feature rather than to the maintenance of it. In this sense its role seems to be secondary compared to the orographic effect.

(e) The influence of the model's "physics" is less clear, as could be expected from general considerations on the profound non-linearity of the model used and of its internal interactions. An almost completely adiabatic model seems able to produce a blocking feature in a similar position, albeit different in several respects. The simultaneous absence, in the model, of surface diabatic forcing and of internal, essentially dissipative, condensation effects, seems to generate a situation in which these two error sources compensate, to a point, ech other, at least in the early part of the simulation.

(f) The role of the Rockies and of their finite latitudinal extent has been investigated further by means of the analysis of the equivalent barotropic vorticity equation and geostrophic eddy momentum flux equation and it has been shown that a possible net effect is to promote a field of momentum flux in the lee of the mountain that leads to a split of the westerlies. This is shown to be consistent with the numerical experiments and with previous results reported in the literature.

**Acknowledgements**

We are indebted to A.Simmons for reading an early version of the manuscript and for several constructive criticisms.

**REFERENCES**


Berggren, K., Bolin, B. and Rossby, C.G. 1949 An aerological study of zonal motion, its perturbation and break down. Tellus, 1, 14-37.

Bengtsson, L. 1979 Review of theories for blocking. European Centre for Medium Range Weather Forecasts, Seminar on Dynamical Meteorology and Numerical Weather Prediction. Vol.2, 235-269.

Bengtsson, L. 1981 Numerical prediction of atmospheric blocking - A case study. Tellus, 33, 19-42.

Burridge, D.M. and Haseler, J. 1977 A model for medium range weather forecasting. European Centre for Medium Range Weather Forecasts, Tech.Rep.No.4, 45 pp.

Charney, J. and de Vore, J. 1979 Multiple flow equilibrium in the atmosphere and blocking. J.Atmos.Sci., 36, 1205-1216.

Chen, Q.S. 1980 The mountain effects on the baroclinic instability of the long and ultra-long waves in the atmosphere. Acta.Meteor.Sinica, 38, 1-15.

Everson, P.J. and Davies, D.R. 1970 On the use of a simple two-level model in general circulation studies. Quart.J.Roy.Met.Soc., 96, 404-412.

Egger, J. 1978 Dynamics of blocking highs. J.Atmos.Sci., 35, 1788-1801.

Green, J.S.A. 1977 The weather during July 1976: Some dynamical considerations on the draught. Weather, 32, 120-126.

Hansen, A.R. and Chen, T.C. 1982 A spectral energetics analysis of atmospheric blocking. Submitted to Mon.Wea.Rev.

Hollingsworth,A., Arpe,K., Tiedtke,M., Capaldo,M. and Savijärvi,H. 1980 The performance of a medium-range forecast model in winter. Impact of physical parameterizations. Mon.Wea.Rev., 108, 1736-1773.

Kikuchi, Y. 1971. Influence of mountains and land-sea distribution on blocking action. J.Met.Soc.Japan, 49, Special Issue, 564-572.

Källén, E. 1981 The nonlinear effects of orogaphic and momentum forcing in a low-order, barotropic model. J.Atmos.Sci., 38, 2150-2163.

Kalnay-Rivas, E. and Merkine, L.O. 1981 A simple mechanism for blocking. J.Atmos.Sci., 38, 2077-2091.

Lorenz, E.N. 1960 Maximum simplification of the dynamic equations. Tellus, 12, 243-254.

Malguzzi, P. and Speranza, A. 1981 Local multiple equilibria and regional atmospheric blocking. J.Atmos.Sci., 38, 1939-1948.

Namias, J. 1964 Seasonal persistence and recurrence of European blocking during 1958-1960. Tellus, 16, 394-407.

Rex, D.F. 1950a. Blocking action in the middle troposphere and its effect upon regional climate. I. An aerological study of blocking action. Tellus, 2, 196-211.

Rex, D.F. 1950b. Blocking action in the middle troposphere and its effect upon regional climate. II. The climatology of blocking action, Tellus, 2, 275-301.

Rossby, C.G. 1950 On the dynamics of certain types of blocking waves. J.Chin.Geophys.Soc., 2, 1-13.

Sumner, E.J. 1954 A study of blocking in the Atlantic - European sector of the Northern Hemisphere. Quart.J.Roy.Met.Soc., 80, 402-416.

Tibaldi,S. and Ji, L.R. 1982 On the effect of model resolution on numerical simulation of blocking. To appear in Tellus.

Tibaldi, S. and Buzzi, A. 1982 Orographic influences on Mediterranean lee cyclogenesis and European blocking in global numerical model. ECMWF Tech.Rep.No.29, 45pp.

Tiedtke, M., J.-F.Geleyn, A.Hollingsworth and J.-F.Louis 1979 ECMWF model-parameterization of sub-grid scale processes. ECMWF Tech.Rep.No.10, 46pp.

Tung, K.K. and Lindzen, R.S. 1979 A theory of stationary long waves. Part I: A simple theory of blocking. Mon.Wea.Rev., 107, 714-734.

Wiin-Nielsen, A., Brown, J.A. and Drake, M. 1963 On atmospheric energy conversions between the zonal flow and the eddies. Tellus, 15, 261-279.

White, W.B. and Clark, N.E. 1975 On the development of blocking ridge activity over the central North Pacific. J.Atmos.Sci., 32, 489-502.

Yeh, T.C. 1949 On energy dispersion in the atmosphere. J.Meteor., 6, 1-16.

Yeh, T.C. and collaborators 1962 Studies on the blocking situations of Northern Hemisphere in Winter. Science Press, Peking. pp.135.

ECMWF PUBLISHED TECHNICAL REPORTS

No. 1 A Case Study of a Ten Day Prediction

No. 2 The Effect of Arithmetic Precisions on some Meteorological Integrations

No. 3 Mixed-Radix Fast Fourier Transforms without Reordering

No. 4 A Model for Medium-Range Weather Forecasting - Adiabatic Formulation

No. 5 A Study of some Parameterizations of Sub-Grid Processes in a Baroclinic Wave in a Two-Dimensional Model

No. 6 The ECMWF Analysis and Data Assimilation Scheme - Analysis of Mass and Wind Fields

No. 7 A Ten Day High Resolution Non-Adiabatic Spectral Integration: A Comparative Study

No. 8 On the Asymptotic Behaviour of Simple Stochastic-Dynamic Systems

No. 9 On Balance Requirements as Initial Conditions

No.10 ECMWF Model - Parameterization of Sub-Grid Processes

No.11 Normal Mode Initialization for a multi-level Gridpoint Model

No.12 Data Assimilation Experiments

No.13 Comparison of Medium Range Forecasts made with two Parameterization Schemes

No.14 On Initial Conditions for Non-Hydrostatic Models

No.15 Adiabatic Formulation and Organization of ECMWF's Spectral Model

No.16 Model Studies of a Developing Boundary Layer over the Ocean

No.17 The Response of a Global Barotropic Model to Forcing by Large-Scale Orography

No.18 Confidence Limits for Verification and Energetics Studies

No.19 A Low Order Barotropic Model on the Sphere with the Orographic and Newtonian Forcing

No.20 A Review of the Normal Mode Initialization Method

No.21 The Adjoint Equation Technique Applied to Meteorological Problems

No.22 The Use of Empirical Methods for Mesoscale Pressure Forecasts

No.23 Comparison of Medium Range Forecasts made with Models using Spectral or Finite Difference Techniques in the Horizontal

No.24 On the Average Errors of an Ensemble of Forecasts

No.25 On the Atmospheric Factors Affecting the Levantine Sea

No.26 Tropical Influences on Stationary Wave Motion in Middle and High Latitudes

ECMWF PUBLISHED TECHNICAL REPORTS

No.27 The Energy Budgets in North America, North Atlantic and Europe Based on ECMWF Analyses and Forecasts

No.28 An Energy and Angular-Momentum Conserving Vertical Finite-Difference Scheme, Hybrid Coordinates, and Medium-Range Weather Prediction

No.29 Orographic Influences on Mediterranean Lee Cyclogenesis and European Blocking in a Global Numerical Model

No.30 Review and Re-assessment of ECNET - a private network with Open Architecture

No.31 An Investigation of the Impact at Middle and High Latitudes of Tropical Forecast Errors

No.32 Short and Medium Range Forecast Differences Between a Spectral and Grid Point Model. An Extensive Quasi-Operational Comparison

No.33 Numerical Simulations of a Case of Blocking: The Effects of Orography and Land-Sea Contrast